THE PENNSYLVANIA STATE UNIVERSITY
SCHREYER HONORS COLLEGE

DEPARTMENT OF CHEMICAL ENGINEERING

UNDERSTANDING THE ROLE OF Te AND Nb IN $MoVTeNbO_x$ FOR OXIDATIVE DEHYDROGENATION OF ETHANE

ABIGAIL IDICULLA
SPRING 2024

A thesis
submitted in partial fulfillment
of the requirements
for baccalaureate degrees
in Civil Engineering
with honors in Chemical Engineering

Reviewed and approved* by the following:

Michael Janik
Professor of Chemical Engineering
Thesis Supervisor

Gina Noh
Assistant Professor of Chemical Engineering
Honors Adviser

*Signatures are on file in the Schreyer Honors College.

Abstract

This thesis investigates the influence of tellurium (Te) and niobium (Nb) on the structure and catalytic performance of $MoVTeNbO_x$ catalysts in the oxidative dehydrogenation of ethane (ODHE). Through comprehensive experimentation, including catalyst preparation, characterization, and performance assessments, we elucidated the optimal molar ratios of Te and Nb that enhance the formation of the M1 phase, crucial for efficient ethylene production. Our findings reveal that a range of Te content (Te:Mo=0.10-0.15) is essential for M1 phase formation without leading to less active phase impurities, such as $TeMo_5O_{16}$, whereas Nb enhances the stability of the M1 phase, indirectly affecting the catalyst's selectivity towards ethylene by spatially isolating active sites and promoting rapid desorption of the desired products. The synthesis procedure, characterized by specific molar ratios of Te and Nb to Mo, significantly influences the formation of the M1 phase, demonstrating that controlled catalyst composition is key to optimal ODHE performance. The study highlights the detrimental effects of excessive Te, leading to the formation of impure phases that negatively impact the catalyst's effectiveness. This research not only advances our understanding of the complex interplay between catalyst composition, structure, and activity in $MoVTeNbO_x$ catalysts but also lays the groundwork for the development of more efficient catalysts for ODHE, offering pathways to more sustainable and cost-effective ethylene production methods.

Table of Contents

List of Figures

List of Tables

Acknowledgements

I would like Professor Gina Noh for taking in me into her lab when I knew nothing about chemical engineering and for teaching me scientific and life lessons to prepare me for graduate school. I also want to thank Brendan Troesch who always helped me, whether it was teaching me chemistry, explaining the project to me, or just talking to me. I thank everyone in the Noh Lab: Sathya, Musa, Winters, Kaiyuan, Nirenjan, and Kathryn. I have enjoyed working with everyone as they made me feel like a real scientist. Special shout-out to Deirdre for being my best friend over the summer. We will always miss you in lab! And finally, thank you to my family, Jacob, and friends for supporting me throughout college and my thesis. I love my entire family, including Koda and Cleo!

Chapter 1

Introduction

1.1 Current Ethylene Production

Ethylene—with a molecular formula of C_2H_4 and one carbon-carbon double bond—is an important industrial organic chemical. The polymerization of ethylene gives polyethylene, a polymer that has many uses, particularly in the production of packaging films, wire coatings, and squeeze bottles. Besides polyethylene, ethylene is the starting material for the preparation of several two-carbon compounds like ethanol, ethylene oxide, acetaldehyde, and vinyl chloride. These substances have a wide range of applications, including in textiles, detergents, and antifreeze. Due to the role of ethylene as a key building block in the production of other chemicals and materials, the demand for ethylene in the United States is expected to increase by 4.1% in 2024, reaching approximately 37.7 million metric tons [1].

The primary process for ethylene production is steam cracking, which is energy-intensive and unselective. Steam cracking is a pyrolysis reaction that involves the decomposition of a hydrocarbon feedstock to produce smaller molecules at high temperatures. Typically, the feedstock includes ethane (C_2H_6) or naphtha derived from petroleum or natural gas, which is then, in the presence of steam and the absence of oxygen, heated to temperatures in the range of 750-950°C. The reactions in steam cracking are highly endothermic. As a result, the process consumes 8% of the global chemical industry's energy consumption [2], making it one of the most energy-intensive processes in the petrochemical industry [3]. Steam cracking results in the emission of 1-2 tons of carbon dioxide (CO_2) per ton of ethylene produced [4]. The majority ($\sim$80%) of this CO_2 is produced by burning fossil fuels in the cracking furnace to achieve the necessary high temperatures [4]. The remainder of the CO_2 emissions are attributed to the use of electricity and heat [4]. In addition to being energy-intensive, steam cracking is not selective to ethylene. During the steam cracking process, C-C bonds in feed molecules break to produce free radicals. Next, the free radical removes a hydrogen atom from another molecule and turns that molecule into a free radical. These radicals can participate in decomposition and addition reactions. In a decomposition reaction, the free radical breaks into two molecules (an alkene and a free radical). In the addition reaction, the radical reacts with an alkene to form a single, heavier free radical. The reaction terminates when two radicals combine to form one larger molecule or when one radical transfers a hydrogen atom to the other. Depending on the composition of the feedstock, steam cracking can produce a variety of products (light olefins, C4 hydrocarbons, and C5 hydrocarbons). Some free radicals may go through thermodynamically favorable reactions to form solid carbonaceous deposits that are referred to as coke. Coking is an undesired side effect of the steam cracking process as it can foul cracking furnaces and heat exchangers, leading to higher pressure drop over the reactor, increased heat-transfer resistance, and periodic shutdowns for cleaning and maintenance [5].

Besides steam cracking, ethylene is also produced by dehydrogenation of ethane, an endothermic reaction. In the dehydrogenation of ethane, hydrogen atoms are removed from ethane to form ethylene with the help of a catalyst, such as platinum, chromium, or aluminum-based catalysts. However, this reaction (Equation 1.1) is difficult due to the strength of the C–H bond of $\sim$101 kcal mol^{-1}, extraordinarily high pKa in the range of 50, and accumulation of hydrogen [6]. To overcome these barriers, high temperatures (550-700°C) must be used, resulting in coke poisoning and catalyst deactivation [7].

$$C_2H_6 \rightleftharpoons C_2H_4 + H_2,\ \Delta_r H_{298} = 136\ \frac{kJ}{mol} \tag{1.1}$$

1.2 Oxidative Dehydrogenation of Ethane

A promising alternative to steam cracking is oxidative dehydrogenation of ethane (ODHE). ODHE is an exothermic reaction (Equation 1.2) and requires less energy input [8].

$$C_2H_6 + \frac{1}{2}O_2 \rightleftharpoons C_2H_4 + H_2O,\ \Delta_r H_{298} = -105.5\ \frac{kJ}{mol} \tag{1.2}$$

With a standard state enthalpy of reaction of -105.5 kJ mol^{-1} and operating temperature between 300-500°C, ODHE uses significantly less energy than steam cracking [9]. Additionally, the ODHE process typically uses oxygen as its oxidant and only produces three products (ethylene, carbon dioxide, and carbon monoxide (CO)) when compared to the side reactions of the previously mentioned processes (Figure 1.1). The presence of oxygen also suppresses coke formation and extends catalyst life [8]. Even though ODHE presents many advantages compared to steam cracking, oxygen has the potential to over-oxidize ethane into CO_2 and CO, resulting in poor ethylene selectivity [10]. The commercial adoption of ODHE has not yet been realized, primarily because steam cracking remains more economically advantageous. There is a consensus that certain critical criteria must be met for the ODHE process to become viable: long-term stability of the catalyst, ethylene yield exceeding 70%, and ethylene productivity rate greater than 1.0 kg_{C2H4} $kg_{cat^{-1}}$ h^{-1} at temperatures below 500°C [9]. Catalyst performance is one of the factors that limits the application of ODHE.

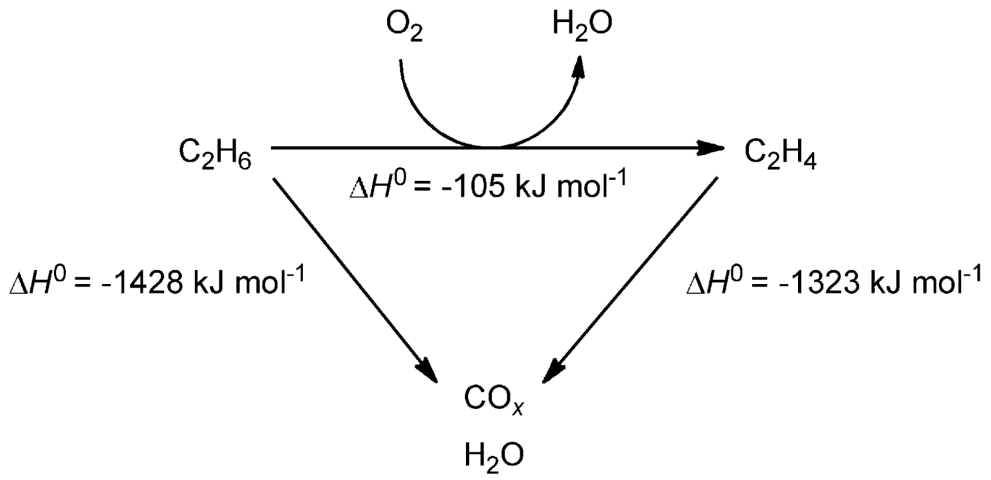

Figure 1.1: Oxidative dehyrogenation of ethane with side reactions using oxygen as the oxidant. Adapted from ref. [8].

1.3 Catalysts for ODHE

Metal oxides are frequently utilized as catalysts in various reactions [11]. They can be categorized into two types: (i) reducible oxides, and (ii) non-reducible oxides [12]. Reducible oxides used for ODHE, such as vanadium oxide (V_2O_5), molybdenum oxide (MoO_3), and iron oxide (Fe_2O), follow a widely accepted Mars–van Krevelen (MvK) mechanism [8]. In the MvK mechanism, ethane

undergoes a reaction with a metal oxide species, leading to the formation of an ethoxy-hydroxy pair. Following this, the β-H atom is activated, resulting in the creation of ethylene which then desorbs from the catalyst, leaving behind a dihydroxy species. Then, the dihydroxy species condense to produce water and leaving being a vacancy, reducing the metal oxide. The now reduced metal oxide is later re-oxidized by oxygen in its gas phase. There is ongoing debate over which oxygen atoms are involved in the initial activation of the C-H bond and the exact configuration of the active site. One theory suggests that ethane may be interacting with oxygen atoms coordinated to a single metal cation. Alternatively, there might be cooperation between two neighboring redox sites or materials, which involves two or more different anions. Non-reducible oxides used for ODHE, including zeolites, alumina (Al_2O_3), and silica (SiO_2), do not undergo significant changes in their oxidation state during the reaction. They facilitate the reaction through different mechanisms, such as acid-base reactions or by providing a surface for the reactants to adsorb and react. Whereas reducible oxide catalyst systems activate ethane at as low as 400°C, non-reducible oxide catalyst systems must operate at elevated temperatures (>600°C) to efficiently facilitate C–H bond activation [13, 14].

1.4 MoVTeNb Oxides for ODHE

In particular, the reducible catalyst consisting of Mo, V, Te, and Nb components has exhibited superior catalytic performance in the ODHE process [9]. This catalyst typically usually consists of M1 (Figure 1.2) and M2 (Figure 1.3) crystalline phases, along with other minor phases like Mo_5O_{14}-type structures and MoV(Te) oxides [15]. M1 is an orthorhombic phase and is built by center-occupied pentagonal rings that are connected by corner-sharing MO_6 octahedrons (M = Mo, V), which are assembled in the (001) plane to form hexagonal and heptagonal rings hosting Te-O units [15]. M2 is a pseudo-hexagonal phase with hexagonal rings hosting the Te-O units without any pentagonal or heptagonal rings in the (001) plane [15]. Previous literature has found the heptagonal micropores in the (001) plane to be responsible for the catalytic activity and the V^{5+} ions to be the active sites for alkane activation [16, 17, 18, 19]. Since only the M1 phase possesses V^{5+} and heptagonal channels, it is the more favorable phase for the ODHE process compared to the M2 phase [17]. Nonetheless, the complex structure and catalytic activity of the $MoVTeNbO_x$ catalyst has led to a contradictory understanding of its properties, posing challenges to the advancement of this catalyst system.

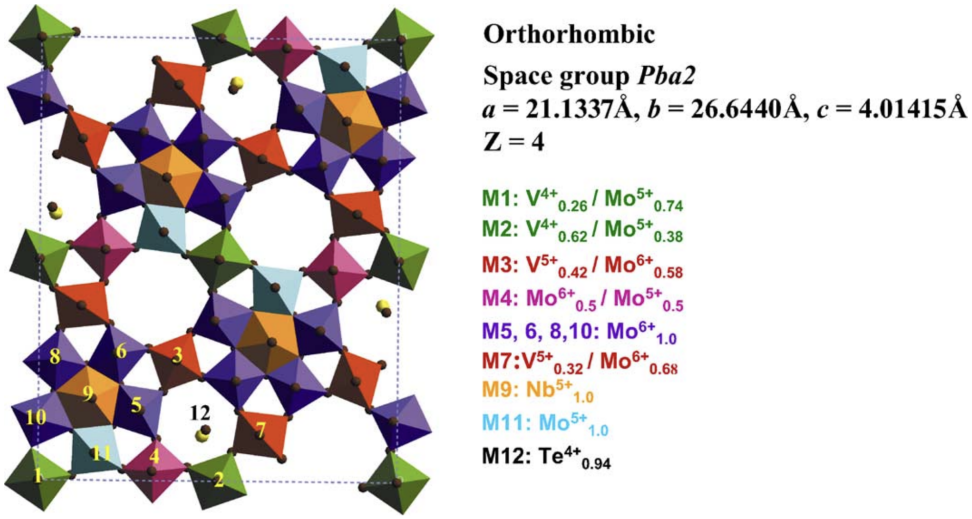

Figure 1.2: Structure of $Mo_{7.8}V_{1.2}NbTe_{0.94}O_{29}$ (M1 phase material). Adapted from ref. [17].

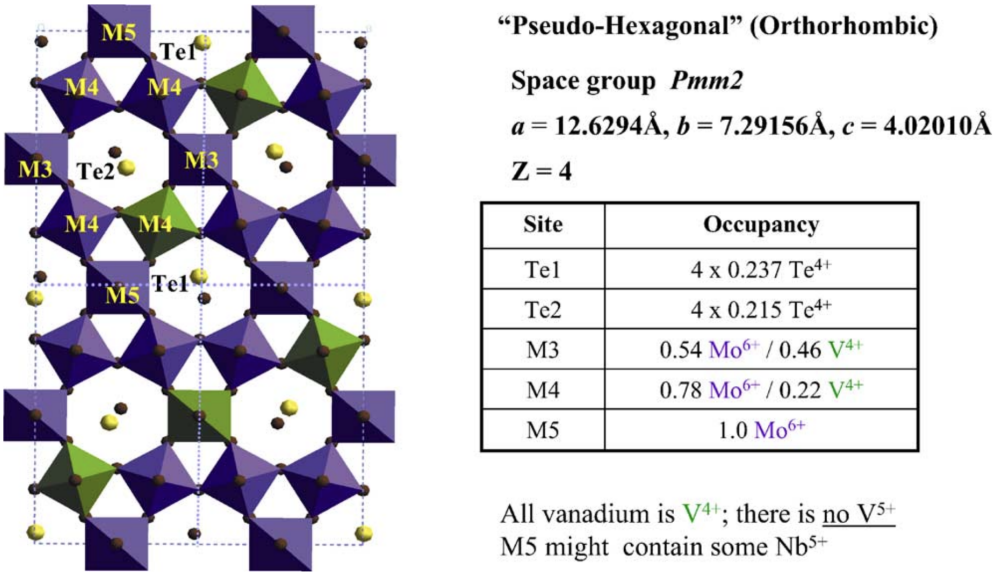

Figure 1.3: Structure of $Mo_{4.67}V_{1.33}Te_{1.82}O_{19.82}$ (M2 phase material). Adapted from ref. [17].

In M1 phase $MoVTeNbO_x$ catalysts, Te plays a role in catalyst structure and oxygen storage in the hexagonal channel [9]. When Te is introduced into the catalyst framework, M1 phase typically forms, making the phase catalytic active in the ODHE process [20]. However, as Te content increases to concentrations not well defined by previous literature, the catalytic activity decreases due to the formation of the impurities (M2 phase and of $TeMo_5O_{16}$) [20]. Low Te concentrations leads to M1 phase formation, whereas high concentrations lead to an excess of Te that cannot be accommodated in the M1 phase [20].

1.5 Current Understanding of the Role of Te in $MoVTeNbO_x$ Catalysts

These Te-containing catalysts are unstable under severe operating conditions due to the sublimation of Te out of the M1 phase, which causes formation of inactive MoO_2 phases. This limits the operating temperature of Te containing M1 catalysts ($<$500°C) and feed composition [9]. Additionally, Te can be reduced from Te^{4+} to form Te^0 on the catalyst surface which blocks the active sites or heptagonal channels resulting in the higher rate of deactivation with time [15].

Ueda et al. claims Te does not affect the oxidation activity of the Mo–V–O framework because Te occupies the central position of the hexagonal ring unit without influencing the framework of the Mo and V octahedra [21]. However, teams Chu et al. and Ishikawa have found high concentrations of Te to affect the activity by increasing Te-O unit occupancy in the heptagonal channel of M1 phase (the necessary pathway for ethane to be selectively oxidized to ethylene) [15, 19].

1.6 Current Understanding of the Role of Nb in $MoVTeNbO_x$ Catalysts

Nb, in M1 phase $MoVTeNbO_x$ catalysts, spatially separates the active sites from each other and stabilizes the M1 phase structure [17]. Nb^{5+} bipyramids, each surrounded by five Mo-O octahedra, spatially isolate the V^{5+} active sites in the (001) plane from each other, preventing the deep oxidation of ethane and ethylene to carbon oxides [15, 22]. Chu et al. and Ueda et al. add that Nb species can promote rapid desorption of the desired products to prevent further oxidation and increase selectivity [15, 23, 21].

Nb content can impact ethylene selectivity in the ODHE process, and a crucial concentration ($MoVTeNb_yO_x$; $y \geq 0.1$) is needed for the stabilization of the M1 phase [20]. As long as a minimum of niobium is contained in the synthesis mixture, the concentration of niobium in the synthesis mixture is not relevant for the formation of the M1 phase [20]. Excess Nb concentrations leads to M1 phase but with an increased amount of amorphous material as Nb changes octahedra arrangement in the M1 phase structure [20]. The distorted octahedra and higher concentration of Nb cations not surrounded by oxygen increases surface residence time by the strong interactions with the reacting molecules [20].

Chapter 2

Methods and Materials

2.1 Catalyst Preparation

$MoVTeNbO_x$ materials were prepared using the following procedure. As an example, to synthesize $MoV_{0.30}Te_{0.15}Nb_{0.15}O_x$, 1.5296 g of ammonium heptamolybdate $(NH_4)_6Mo_7O_{24}•4H_2O$ (Sigma-Aldrich, 99.98% purity) was dissolved in 17 mL deionized (DI) water so that the final 25 mL solution had a Mo concentration of 0.5 mol L^{-1}. Then, the solution was heated on a hot plate to 80°C and stirred for 10 minutes at 450 rpm. Next, 0.6586 g of powder vanadyl sulfate $VOSO_4•5H_2O$ (Sigma-Aldrich, 97% purity) was mixed into the aqueous solution and stirred for 10 minutes, followed by 0.2998 g of powder telluric acid $Te(OH)_6$ (Thermo, >99% purity) and stirred for another 10 minutes. Separately, 0.5109 g of ammonium niobate oxalate $(NH_4)[NbO(C_2O_4)_2(H_2O)_2]•3H_2O$ (Sigma-Aldrich, 99.99% purity) was dissolved in DI water at 40°C. Before adding the ammonium niobate oxalate solution to the ternary ammonium paramolybdate, vanadyl sulfate, and telluric acid solution, the latter's hot plate temperature was lowered to 40°C. Once the temperature stabilized at 40°C, the two solutions were mixed and stirred for 10 minutes at 550 rpm. The final solution had a pH of ∼3 using Mettler Toledo pH Sensor InLab® Max Pro-ISM.

The solution was transferred to a Teflon liner (40 mL) placed inside of a stainless-steel Parr, then sealed and placed in an oven heated to 175°C for 48 hours. After taking out and cooling the solution, the solution was transferred to a 50 mL Falcon® Conical Centrifuge Tube, DI water was added until the tube was 2/3 full, and the mixture was centrifuged for 10 minutes at 11,360 rpm. Then, the supernatant was discarded, and the solids were dried at 85°C in stagnant air for 12 hours. The dried solids were then annealed under flowing N_2 via heating at 100°C h^{-1} until it reached 600°C, allowing the product to dwell at 600°C for 2 hours, and then cooling at 50°C hr^{-1} until ambient temperature.

To obtain varying Te/Mo and Nb/Mo molar ratios, the mass of telluric acid dihydrate and ammonium niobate oxalate hydrate were adjusted accordingly while the mass of ammonium paramolybdate tetrahydrate and vanadyl sulfate pentahydrate were held constant (Table 2.1).

Sample	Nominal Composition (Mo:V:Te:Nb)
$Te_{0.15}Nb_{0.15}$-M1	1:0.30:0.15:0.15
$Te_{0.20}Nb_{0.20}$-M1	1:0.30:0.20:0.20
$Te_{0.20}Nb_{0.15}$-M1	1:0.30:0.20:0.15
$Te_{0.15}Nb_{0.20}$-M1	1:0.30:0.15:0.20
$Te_{0.10}Nb_{0.10}$-M1	1:0.30:0.10:0.10
$Te_{0.05}Nb_{0.05}$-T	1:0.30:0.05:0.05
$Te_{0.10}Nb_{0.05}$-M1	1:0.30:0.10:0.05
$Te_{0.05}Nb_{0.10}$-T	1:0.30:0.05:0.10
$Te_{0.20}Nb_{0.05}$-M	1:0.30:0.20:0.05
$Te_{0.15}Nb_{0.05}$-M	1:0.30:0.15:0.05
$Te_{0.20}Nb_{0.10}$-M	1:0.30:0.20:0.10
$Te_{0.15}Nb_{0.10}$-M1	1:0.30:0.15:0.10
$Te_{0.05}Nb_{0.15}$-T	1:0.30:0.05:0.15
$Te_{0.05}Nb_{0.20}$-T	1:0.30:0.05:0.20
$Te_{0.10}Nb_{0.15}$-M1	1:0.30:0.10:0.15
$Te_{0.10}Nb_{0.20}$-T	1:0.30:0.10:0.20

Table 2.1: $MoVTeNbO_x$ catalyst samples and their as-synthesized compositions, given as molar ratios of V, Te, or Nb with respect to Mo

2.2 Catalyst Characterization

Before and after annealing, the material was characterized using X-ray diffraction (XRD) (Bruker D2 Phaser). The scanning rate used was 0.125 seconds per step for 2472 steps, and the scanning range (2θ) was 5°to 55°. Following XRD, the material was pressed (3.75 tons for 3 minutes), gently crushed, and sieved to retain aggregates between 180-250 μm in size.

2.3 Catalytic Activity, Selectivity, and Rate Measurements

For each material, the reaction rates were measured at 300°C, 350°C, and 400°C using a fixed bed plug flow reactor. Temperatures were maintained with a three-zone resistively heated furnace (Applied Test Systems Series 3210-200-8-18) using electronic controllers (Watlow EZ-ZONE PM) and measured with a K-type thermocouple axially aligned with the mid-point of the packed bed. Before inserting the catalyst into the reactor, glass wool was inserted in the reactor to prevent the catalyst from moving. Additionally, the 180 μm fines were diluted with 120 mg of calcined silica to distribute heat throughout the catalyst bed. The catalyst-silica mixture was inserted into the reactor, which was then stuffed with more glass wool. Before initiating the reaction, 73 standard cm^3 min^{-1} (sccm) N_2 flowed over the catalyst bed as the furnace temperature ramped up to 450°C at 15°C per

minute. After dwelling for an hour, the furnace temperature was adjusted until the thermocouple in the reactor read the desired reaction temperature. Once at the reaction temperature, the feed, which consisted of ethane (99% C_2H_6, 1% H_2O, N_2, O_2, CO_2+CO, and other hydrocarbons), air (20% O_2, 80% N_2), and N_2 purchased from Praxair and Linde, was controlled using Parker Hannifin Corporation Porter Instrument Series II Digital Mass Flow Controllers. The feed gas composition was fixed at 10% ethane, 10% O_2, and 80% N_2 (1:1:8 of C_2H_6:O_2:N_2). The total flow rate of feed gas was changed every six injections to vary the weight hourly space velocity (WHSV). For $MoV_{0.30}Te_{0.15}Nb_{0.15}O_x$, the WHSV changed from 6.63x10^{-6}, 1.63x10^{-5}, 3.37x10^{-6}, 1.68x10^{-6}, and back to 6.63x10^{-6} cm^3 g^{-1} hr^{-1}.

The composition of the reactor effluent was analyzed using on-line gas chromatography (Agilent 7890B) and thermal conductivity detection (TCD; ShinCarbon ST micropacked 2 m x 1 mm) for CO_2, CO, ethane, and ethylene and flame ionization detection (FID; HP-PLOT/Al_2O_3 50 m x 0.53 mm x 15 m) for ethane and ethylene.

Since the sensitivity of the TCD to organic molecules is lower than the FID, the total reactant pressure was calculated using the normalized areas of methane, ethane, and ethylene from the FID and the normalized areas of CO_2 and CO from the TCD.

For the first six injections, the feed gas was directed away from the reactor bed and straight to the GC to determine the composition of the feed. This percentage of ethane was used to calculate the conversion (Equation 2.1). The selectivity to ethylene was calculated using Equation 2.2. The rates of ethane, ethylene, CO_2, and CO were determined based on Equation 2.3.

$$\text{Conversion}[\%] = \frac{\text{influent ethane}[\%] - \text{effluent ethane}[\text{kPa}]}{\text{influent ethane}[\%]} \tag{2.1}$$

$$\text{Selectivity}[\%] = \frac{\text{effluent ethylene}[\text{kPa}]}{\text{total effluent}[\text{kPa}]} \tag{2.2}$$

$$\text{Rates}\left[\frac{\text{mol}}{\text{g}\cdot\text{s}}\right] = \frac{(\text{effluent ethane}[\%] - \text{influent ethane}[\%]) \times \text{WHSV}\left[\frac{\text{mol}}{\text{g}\cdot\text{s}}\right]}{\text{influent ethane}[\%]} \tag{2.3}$$

Chapter 3

Results and Discussion of Ethane ODH over M1 Oxides

3.1 Introduction

Previous literature has found a good correlation between ODHE catalytic performance and the crystallinity properties of the M1 phase $MoVTeNbO_x$ catalyst [24]. Thus, a phase-pure, highly crystalline M1 $MoVTeNbO_x$ catalyst is ideal for obtaining a high productivity in the ODHE process. As the presence of Te is attributed to M1 formation, and Nb stabilizes the M1 phase, it is important to understand the relationship between the Te and Nb content in $MoVTeNbO_x$ [20, 17]. Varying the Te content can result in the formation of the M2 phase and $TeMo_5O_{16}$ and decrease catalytic activity [20]. While Nb is not necessary for M1 formation, the increasing Nb content can increase amorphous material and alter the selectivity of the catalyst [20]. This chapter characterizes the synthesized catalysts using powder X-ray diffraction (XRD) and reports the catalytic results for ODHE over these samples to analyze the relationship between Te and Nb content and M1 phase crystallinity as well as catalytic performance.

3.2 M1 Phase Characterization

XRD patterns were recorded to understand the relationship between catalyst composition and M1 phase crystallinity. Phase identification of the catalysts was carried out by comparing the collected spectra with those listed in the Inorganic Crystal Structure Database (ICSD). Figure 3.1 shows diffraction patterns for annealed $Te_{0.15}Nb_{0.15}$-M1, $Te_{0.20}Nb_{0.20}$-M1, $Te_{0.20}Nb_{0.15}$-M1, $Te_{0.15}Nb_{0.20}$-M1, and $Te_{0.10}Nb_{0.10}$-M1 materials, and the simulated pattern for the reference M1 phase material (ICSD 55097; [25]). The diffraction patterns indicate the presence of M1 phase.

Using Rietveld Analysis, the crystallinities for $Te_{0.20}Nb_{0.15}$-M1, $Te_{0.15}Nb_{0.20}$-M1, and $Te_{0.10}Nb_{0.10}$-M1 were 66.38%, 89.2%, and 80.92%, respectively. I propose that a sufficient Te content is needed to form crystalline M1 phase catalyst without decomposing into the M2 or $TeMo_5O_{16}$ phases. A deficient amount of Te will inhibit M1 phase formation, but an excessive Te content will result in the formation of other inactive phases. Additionally, a Nb:Mo concentration of $\leq$0.20 is ideal to form a crystalline M1 phase without increasing the amorphous content. After establishing the presence of M1 phase in the $Te_{0.15}Nb_{0.15}$-M1, $Te_{0.20}Nb_{0.20}$-M1, $Te_{0.20}Nb_{0.15}$-M1, $Te_{0.15}Nb_{0.20}$-M1, and $Te_{0.10}Nb_{0.10}$-M1 materials, the catalytic performance of each sample was tested.

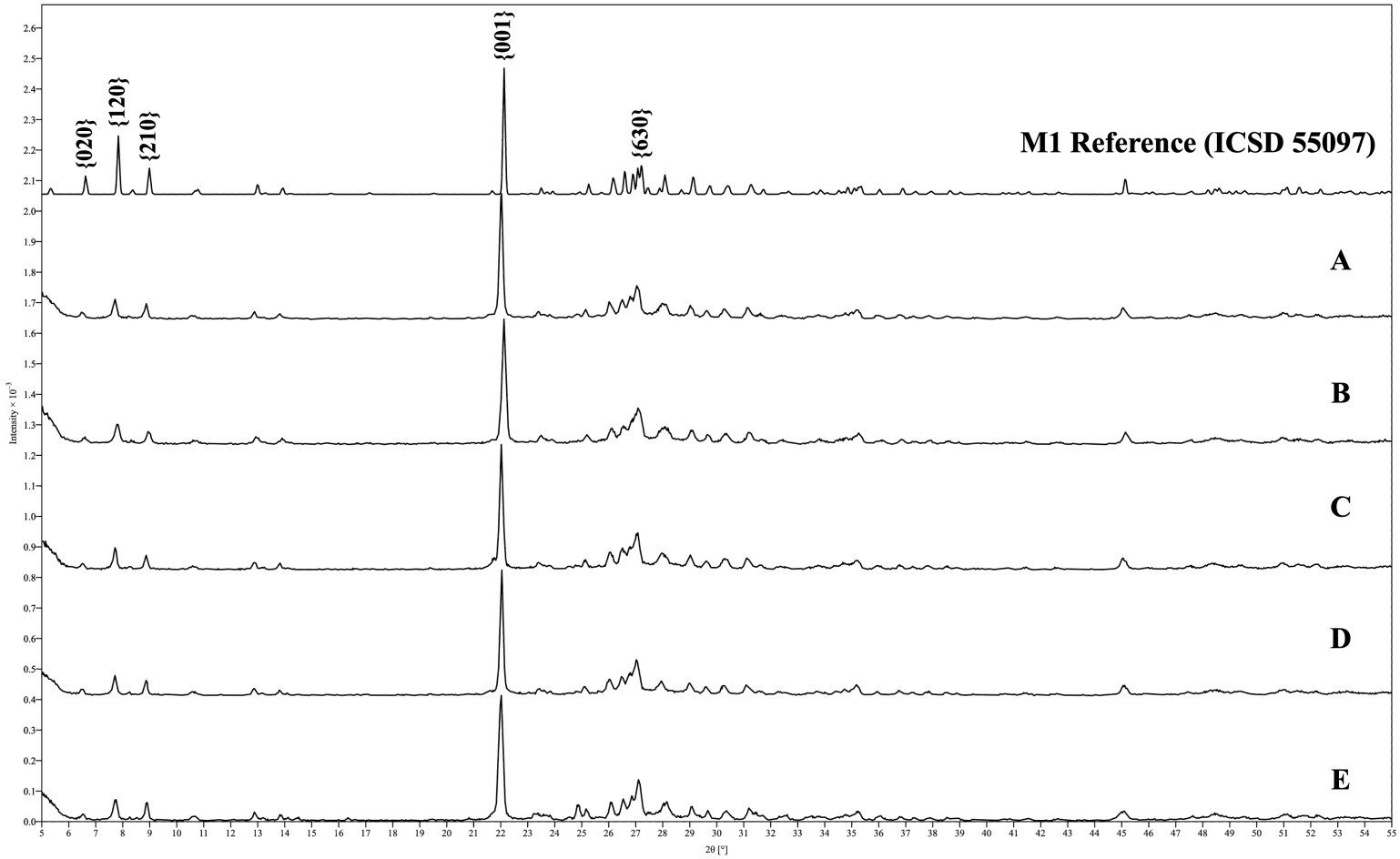

Figure 3.1: XRD patterns of simulated M1 phase (ICSD 55097) as well as annealed $Te_{0.15}Nb_{0.15}$-M1 (A), $Te_{0.20}Nb_{0.20}$-M1 (B), $Te_{0.20}Nb_{0.15}$-M1 (C), $Te_{0.15}Nb_{0.20}$-M1 (D), and $Te_{0.10}Nb_{0.10}$-M1 (E) samples from 2θ=5-55°. M1 phase (ICDS 55097) has characteristic diffraction lines located at 2θ = 6.63, 7.83, 8.99, 22.13, and 27.21°, corresponding to the (020), (120), (210), (001), and (630) crystal directions, respectively.

3.3 Catalytic Results of ODHE Over M1 Phase Samples

Following the catalytic tests, ethane conversion, ethylene selectivity, CO_2 selectivity, CO selectivity, and rates were calculated to better understand the effect of Te and Nb content on M1 phase catalytic activity and selectivity in the ODHE process. Figure 3.2.A plots ethylene selectivity as a function of ethane conversion for $Te_{0.15}Nb_{0.15}$-M1, $Te_{0.20}Nb_{0.20}$-M1, $Te_{0.15}Nb_{0.20}$-M1, and $Te_{0.10}Nb_{0.10}$-M1 materials at 300°C, where ethane conversion was varied by changing residence time. At low conversions (<3%), all materials exhibit 100% selectivity to ethylene. As conversions increase, selectivities to ethylene decrease slightly as selectivity to CO_2 and CO increase to 3% and 0%, respectively. These trends are consistent with expectations that samples ($Te_{0.15}Nb_{0.20}$-M1 and $Te_{0.10}Nb_{0.10}$-M1) with higher crystallinity (>80%) are more active in the ODHE process. Both these samples contain lower amounts of Te, supporting the idea that a lower range of Te content is necessary for crystalline M1 phase formation.

At higher temperatures (350°C), Figure 3.2.B shows higher ethane conversions and lower ethylene selectivities. Due to the high ethane conversion and ethylene selectivity of sample $Te_{0.15}Nb_{0.15}$-M1, a molar ratio of Te:Mo=0.15 seems to be the ideal value for more active M1 phase catalytic performance in the ODHE process. Sample $Te_{0.20}Nb_{0.15}$-M1 displays the lowest ethane conversion, furthering the conclusion that increasing crystallinity improves catalytic performance.

As the temperature increases to 400°C, a similar trend in the materials was seen: ethylene selectivity continues to decrease as ethane conversion increases. While samples $Te_{0.15}Nb_{0.20}$-M1 and $Te_{0.10}Nb_{0.10}$-M1 show the highest catalytic activity, sample $Te_{0.15}Nb_{0.15}$-M1 demonstrates higher ethylene selectivity at similar ethane conversions, supporting the molar ratio of Te:Mo=0.15 as the ideal value for crystalline M1 phase formation. Additionally, Nb:Mo=0.15 might be the ideal molar ratio for site isolation without increasing distorted octahedra and concentration of Nb not surrounded by oxygen, which leads to strong surface interactions with the reacting molecules and increased surface residence time.

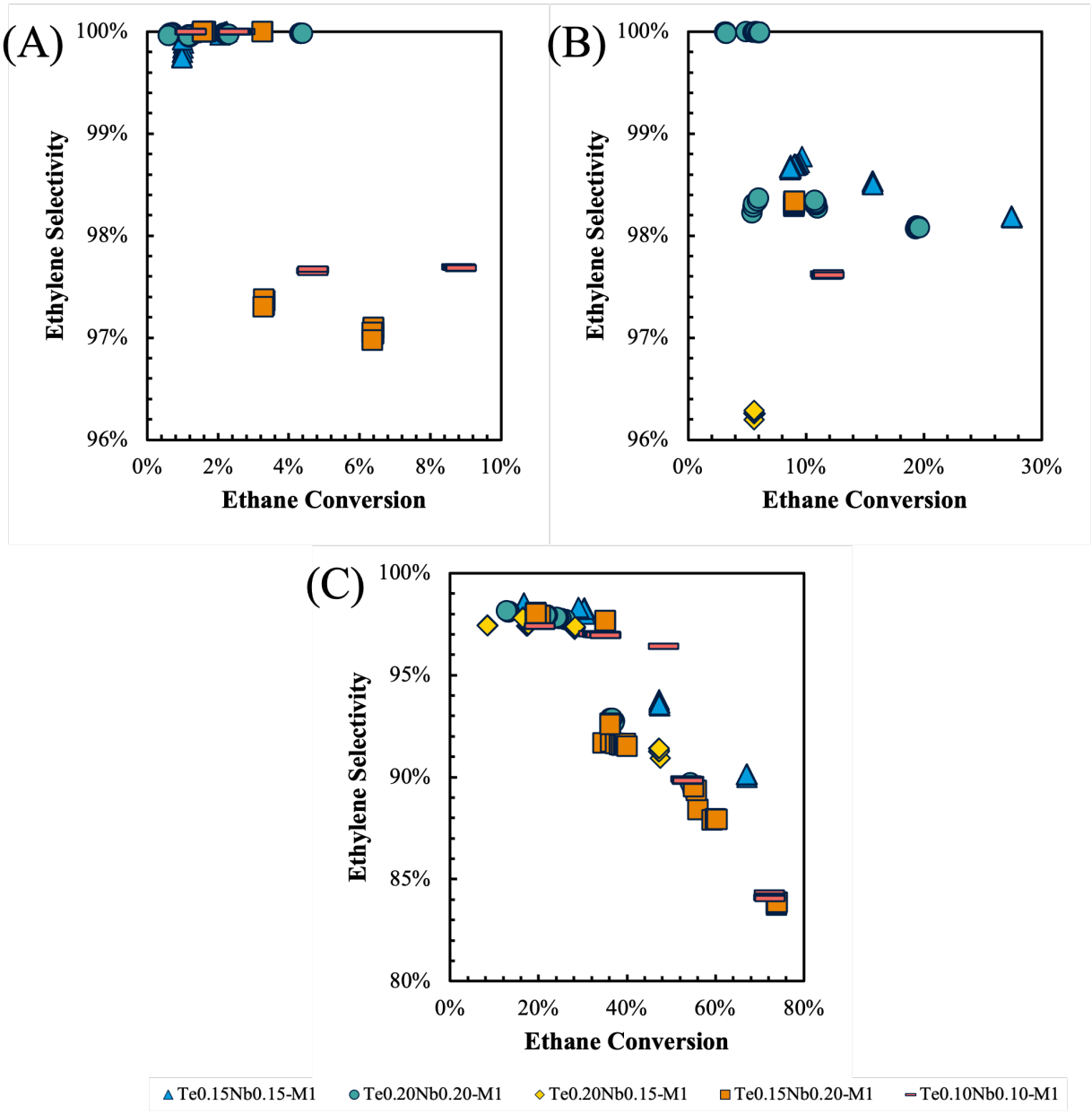

Figure 3.2: Ethylene selectivity as a function of ethane conversion for $Te_{0.15}Nb_{0.15}$-M1 (triangle), $Te_{0.20}Nb_{0.20}$-M1 (circle), $Te_{0.20}Nb_{0.15}$-M1 (diamond), $Te_{0.15}Nb_{0.20}$-M1 (square), and $Te_{0.10}Nb_{0.10}$-M1 (rectangle) sample materials at (A) 300°C, (B) 350°C, and (C) 400°C where ethane conversion was varied by changing residence time at constant ethane and O_2 pressures of 10.13 kPa.

The following figure, Figure 3.3, includes the rate of ethylene formation as a function of ethane conversion. Any significant effects of the residence time on product formation rates (product inhibition) were removed by extrapolating all rates measured at <10% conversions to zero reactant conversion. Therefore, all rates reported reflect ODHE rates at the conditions of the reactor inlet free from all products. All the catalyst samples, except for $Te_{0.15}Nb_{0.20}$-M1, show as ethane conversion increases, the rate of ethylene formation decreases. The initial ethylene formation rate over $Te_{0.10}Nb_{0.10}$-M1 was about a factor of two to three times greater than the other samples.

Initial ethylene formation rates decreased as the Te:Mo molar ratio increased. These results suggest increased catalytic activity over catalysts with Te:Mo less than or equal to 0.15 and that catalytic activity is independent of Nb content as long as M1 phase is present. Previous papers have claimed Te seems to not affect the oxidation activity of the Mo–V–O framework [21], but these results suggest the Te content in M1 phase catalysts has some effect on the activity.

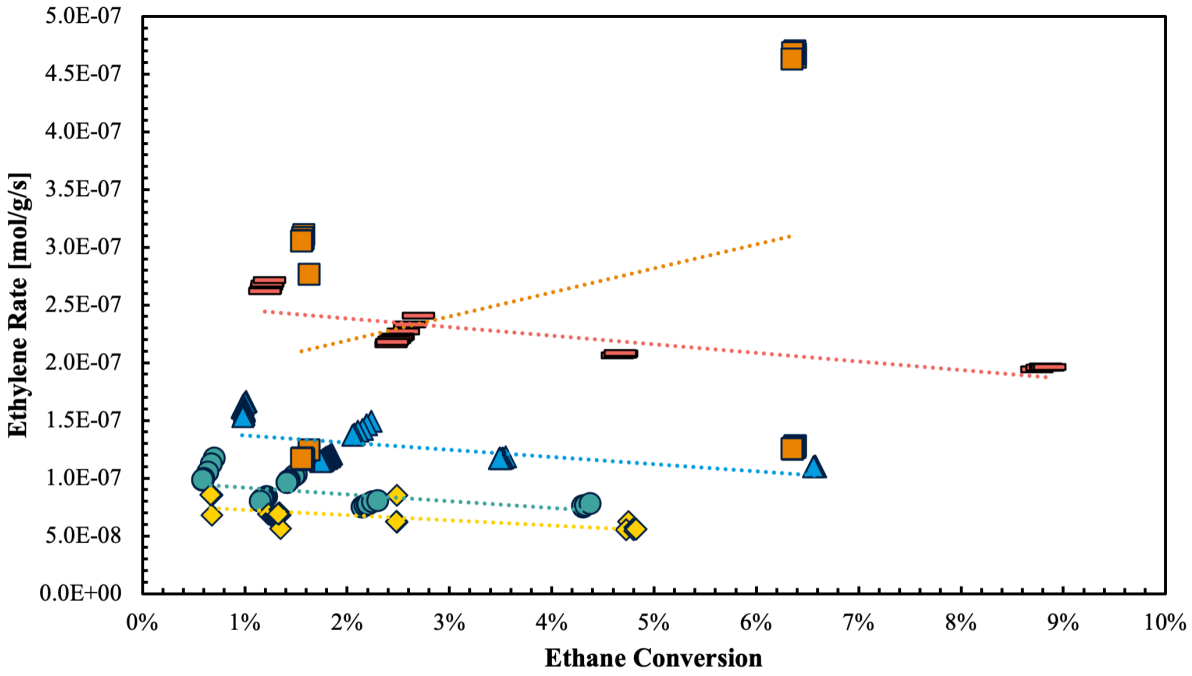

Figure 3.3: Ethylene formation rate as a function of ethane conversion for $Te_{0.15}Nb_{0.15}$-M1 (triangle), $Te_{0.20}Nb_{0.20}$-M1 (circle), $Te_{0.20}Nb_{0.15}$-M1 (diamond), $Te_{0.15}Nb_{0.20}$-M1 (square), and $Te_{0.10}Nb_{0.10}$-M1 (rectangle) sample materials at 300°C. Rates were extrapolated to initial residence times (zero reactant conversion) to account for the significant effects of the residence time on product formation rates.

Figure 3.4 depicts the formation rate of the products ethylene, CO_2, and CO at 300°C. At lower temperatures, the primary product is ethylene and CO_2, but as the temperature increases, the production rate of CO_2 and CO increases. All the materials have different rates; however, this difference is not attributed to different redox abilities of the samples, rather the difference in active site density. So this is likely due to differences in site densities. Ethylene formation rate without CO_2 formation is highest over the $Te_{0.15}Nb_{0.15}$-M1; however, the ethylene formation rate with CO_2 formation is highest over the $Te_{0.15}Nb_{0.20}$-M1 and $Te_{0.10}Nb_{0.10}$-M samples. At 300°C the latter two samples appear to be more active but without the ideal Nb:Mo molar ratio to prevent deeper oxidation of ethylene.

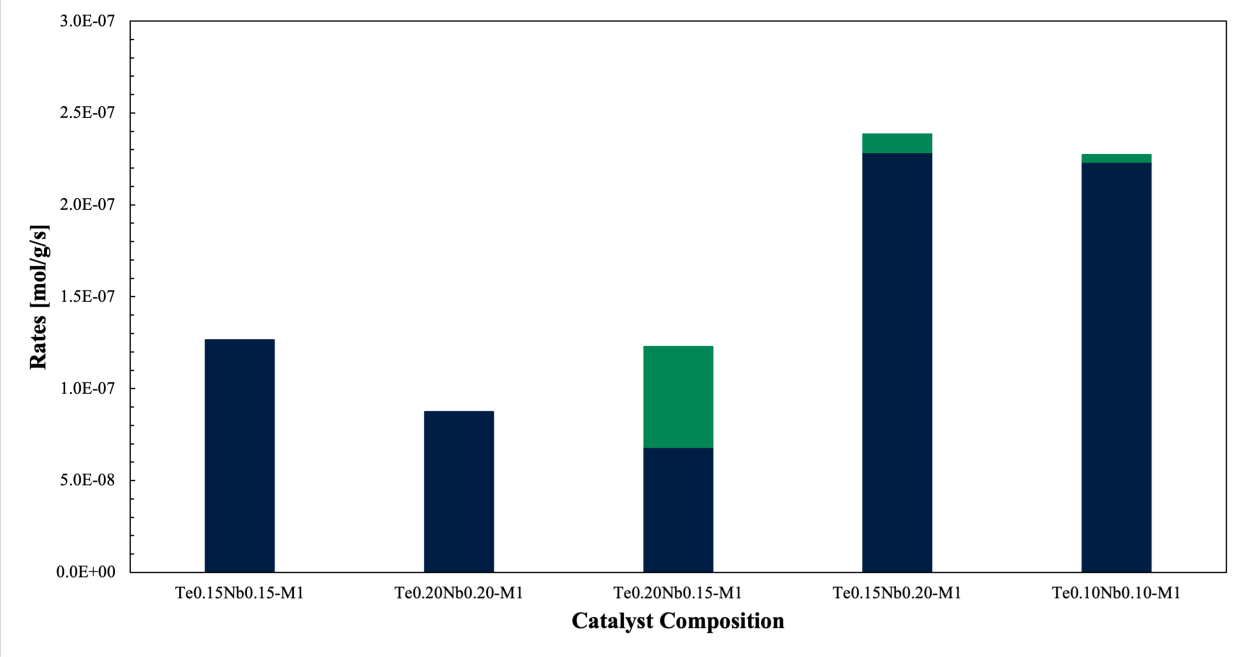

Figure 3.4: Ethylene (dark blue) and CO_2 (green) formation rates over samples $Te_{0.15}Nb_{0.15}$-M1, $Te_{0.20}Nb_{0.20}$-M1, $Te_{0.20}Nb_{0.15}$-M1, $Te_{0.15}Nb_{0.20}$-M1, and $Te_{0.10}Nb_{0.10}$-M1 at 300°C.

3.4 Conclusion

This chapter explored the oxidative dehydrogenation of ethane over M1 oxides, focusing on the role of Te and Nb in the crystalline structure and catalytic performance of the M1 phase catalysts. Through varying ratios of Te and Nb to Mo, it was established that the presence of Te is crucial for M1 phase formation, favoring Te:Mo $\leq$0.15, while Nb aids in stabilizing this phase, thereby influencing the catalyst's performance.

Chapter 4

Results and Discussion of Ethane ODH over Mo_5O_{14} Phase Impure Materials

4.1 Introduction

Depending on the preparation method, different phases may form in MoVTeNb oxide catalysts, such as the ternary $(MoVNb)_5O_{14}$ oxide of the tetragonal Mo_5O_{14}-type structure (ICSD 27202; [26]; [27]). The $(MoVNb)_5O_{14}$ phase contains MO_7 (M = Mo, V, N) pentagonal bipyramids which share all five edges with MO_6 octahedra [28]. The Mo_5O_{14}-type structure is similar to the M1 phase as it has an open structure with channels that may be occupied by different metal cations. Additionally, the local and electronic structure of V is similar in both phases. The partial substitution of V for Mo has been shown to stabilize the binary Mo_5O_{14} [28]. Therefore, the heterogeneous site occupancy must be a necessary condition for its catalytic activity and selectivity. Under oxidizing conditions at temperatures $\geq$723 K, $(MoVNb)_5O_{14}$ decomposed into a MoO_3-type structure [29]. This low redox stability might inhibit structural recovery of the surface, decreasing catalytic performance [29]. Previous literature conflicts on whether mixed metal MoVNb oxides possessing a Mo_5O_{14}-type structure are active for the selective oxidation of ethane [15, 29]. This chapter characterizes the synthesized catalysts using XRD and reports the catalytic results for ODHE over Mo_5O_{14} phase impure materials.

4.2 Tetragonal Mo_5O_{14} Phase Characterization

XRD patterns were recorded to understand the relationship between catalyst composition and the formation of different $MoVTeNbO_x$ phases. Phase identification of the catalysts was carried out by comparing the collected spectra with those listed in the ICSD database. Figure 4.1 shows diffraction patterns for the simulated pattern for the reference M1 phase material (ICSD 55097; [25]) and Mo_5O_{14} phase material (ICSD 27202; [26]) as well as annealed $Te_{0.05}Nb_{0.05}$-T, $Te_{0.05}Nb_{0.10}$-T, $Te_{0.05}Nb_{0.15}$-T, and $Te_{0.10}Nb_{0.20}$-T materials. XRD patterns of these samples suggest the presence of M1 and Mo_5O_{14}-type phases. All synthesized catalysts with a Te:Mo molar ratio of 0.05 displayed similar diffraction patterns to the Mo_5O_{14} reference phase. The low Te content prevents M1 formation and likely leads to the $(MoVNb)_5O_{14}$ impurity due to inadequate Te incorporation into the hexagonal and heptagonal channels. Although Rietveld analysis was not conducted on these materials, as the Nb content increases, the more amorphous the materials appear. This is in agreement with previous literature stating the preferential incorporation of Nb into amorphous material [20]. After understanding the crystallinity and phase composition of the $Te_{0.05}Nb_{0.05}$-T, $Te_{0.05}Nb_{0.10}$-T, $Te_{0.05}Nb_{0.15}$-T, and $Te_{0.10}Nb_{0.20}$-T materials, catalytic tests were performed to understand how the Te and Nb concentrations and $(MoVNb)_5O_{14}$ impurity impacts catalytic performance.

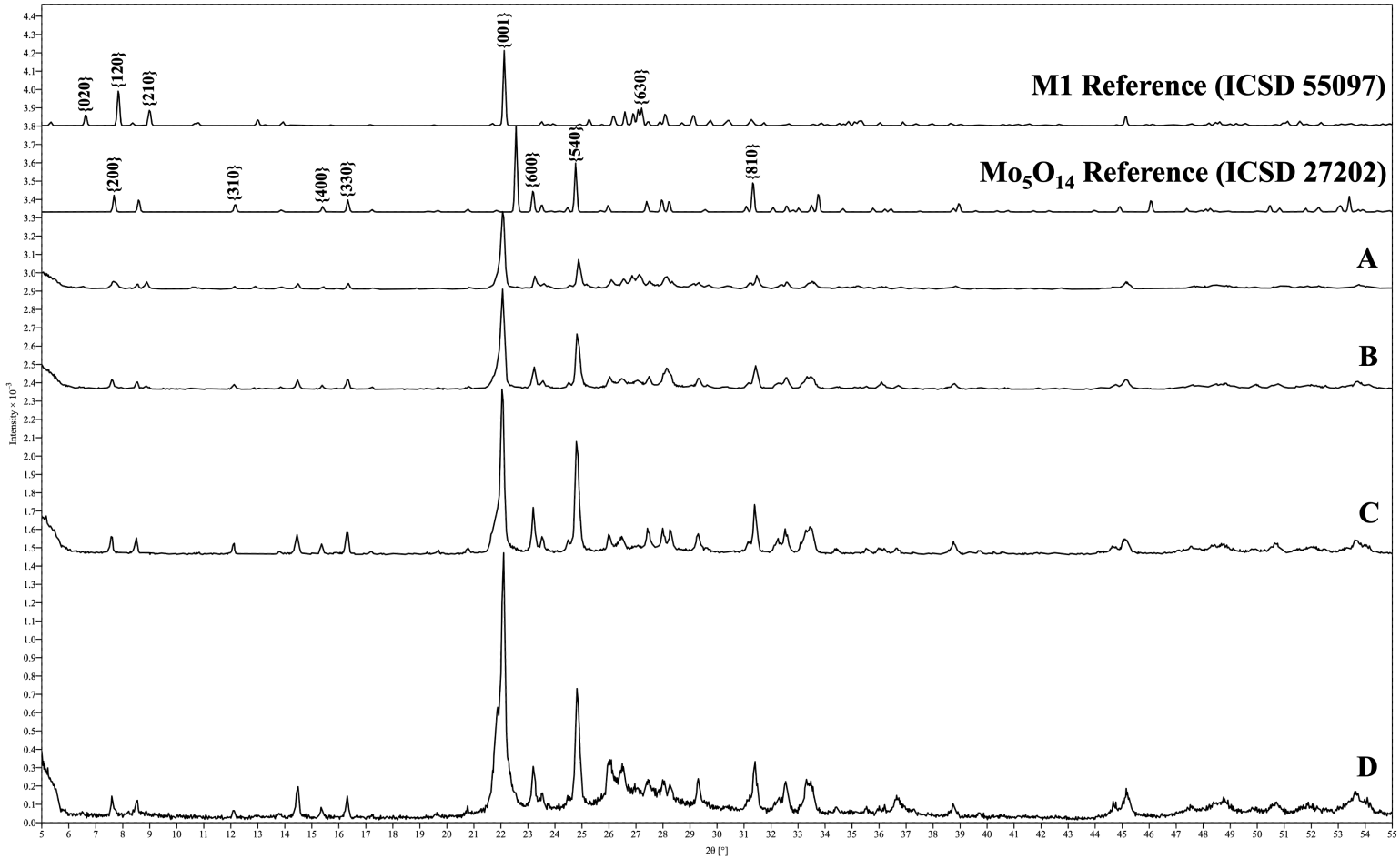

Figure 4.1: XRD patterns of simulated M1 phase (ICSD 55097) and Mo_5O_{14} phase (ICSD 27202) as well as annealed $Te_{0.05}Nb_{0.05}$-T (A), $Te_{0.05}Nb_{0.10}$-T (B), $Te_{0.05}Nb_{0.15}$-T (C), and $Te_{0.10}Nb_{0.20}$-T (D) samples from 2θ=5-55°. M1 phase (ICDS 55097) has characteristic diffraction lines located at 2θ = 6.63, 7.83, 8.99, 22.13, and 27.21°, corresponding to the (020), (120), (210), (001), and (630) crystal directions, respectively. Tetragonal Mo_5O_{14}-type structure has characteristic diffraction lines located at 2θ = 7.68, 12.16, 15.40, 16.34, 23.19, 24.77, and 31.34°, corresponding to the crystal directions (200), (310), (400), (330), (600), (540), and (810), respectively.

4.3 Catalytic Results of ODHE Over Mo_5O_{14} Phase Samples

Following the catalytic tests, ethane conversion, ethylene selectivity, CO_2 selectivity, CO selectivity, and rates were calculated to better understand the effect of Te and Nb content on $(MoVNb)_5O_{14}$ impurity catalytic activity and selectivity in the ODHE process. Figure 4.2.A plots ethylene selectivity as a function of ethane conversion for $Te_{0.05}Nb_{0.05}$-T, $Te_{0.05}Nb_{0.01}$-T, $Te_{0.05}Nb_{0.15}$-T, and $Te_{0.10}Nb_{0.20}$-T materials at 300°C, where ethane conversion was varied by changing residence time. At low conversions (¡ 2%), all materials exhibit 100% selectivity to ethylene. As conversions increase, selectivities to ethylene decrease slightly. At higher temperatures (350°C and 400°C), Figures 4.2.B and C show higher ethane conversions and lower ethylene selectivities, consistent with the catalytic results in Chapter 3. Sample $Te_{0.05}Nb_{0.05}$-T continues to demonstrate the highest ethane conversions (13% at 350°C and 80% at 400°C) and ethylene selectivities (98% at 350°C and 78% at 400°C). These ethane conversions are similar to the catalytic activity of sample $Te_{0.15}Nb_{0.20}$-M1, but these ethylene selectivities are lower than those of the aforementioned M1 sample. Overall, the $(MoVNb)_5O_{14}$ phase samples have lower ethane conversions and ethylene selectivites compared to the M1 phase samples.

The $Te_{0.05}Nb_{0.05}$-T, $Te_{0.05}Nb_{0.01}$-T, and $Te_{0.05}Nb_{0.15}$-T samples contain the lowest Te content of all synthesized catalyst samples. The poor incorporation of Te into the $(MoVNb)_5O_{14}$ framework suggests Te plays a dominant role in the M1 phase distribution of the final catalyst and improves catalytic activity. Furthermore, the results showed that the Te-O_x chains in the hexagonal channels might be involved in the redox of the catalyst and the re-oxidation of the active sites on the surface, which suggests the hexagonal channels act as oxygen reservoirs in the ODHE process. The $Te_{0.05}Nb_{0.05}$-T, $Te_{0.05}Nb_{0.01}$-T, $Te_{0.05}Nb_{0.15}$-T, and $Te_{0.10}Nb_{0.20}$-T samples all have varying Nb concentrations, further supporting Nb does not participate in the reaction.

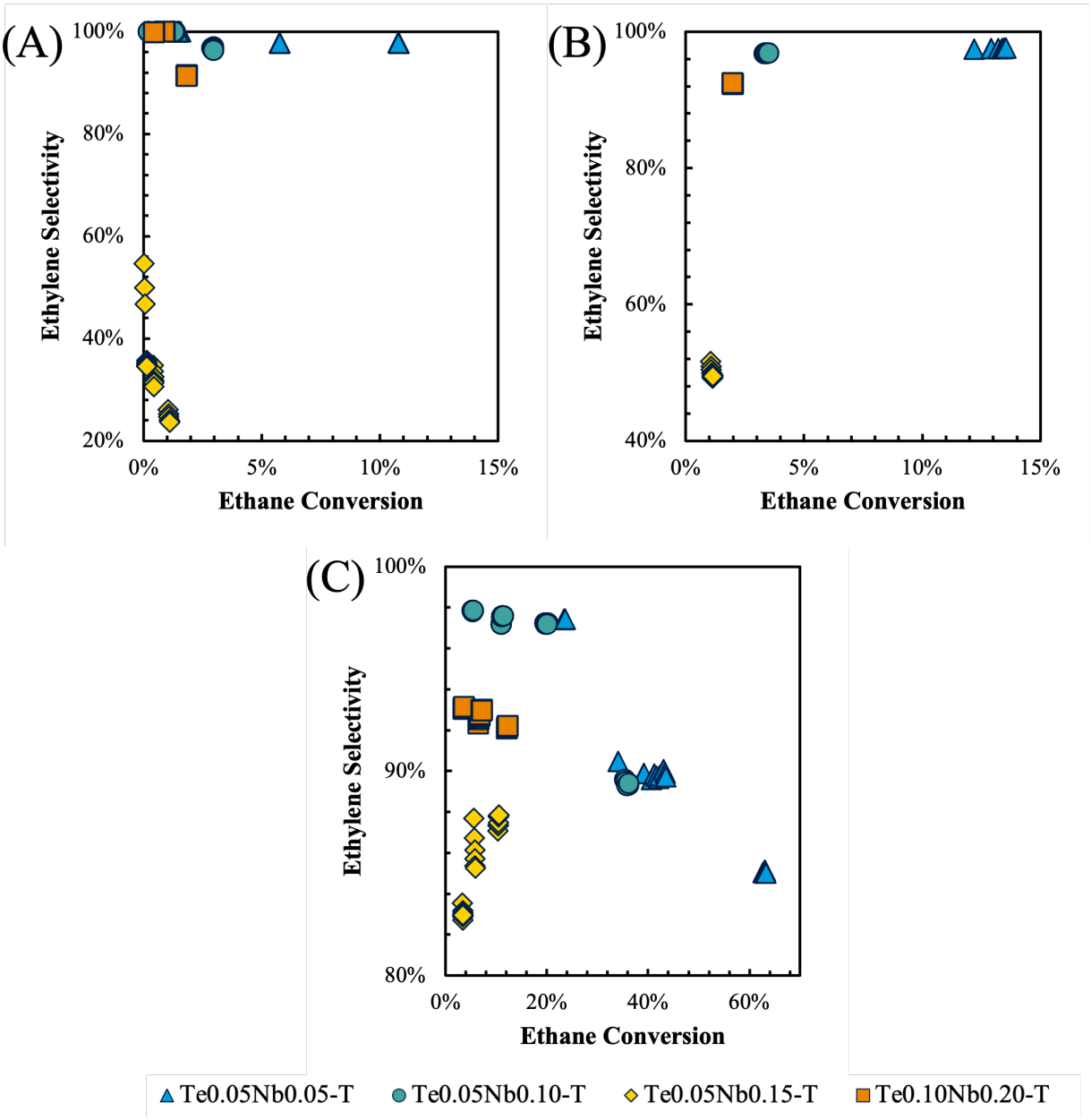

Figure 4.2: Ethylene selectivity as a function of ethane conversion for $Te_{0.05}Nb_{0.05}$-T (triangle), $Te_{0.05}Nb_{0.01}$-T (circle), $Te_{0.05}Nb_{0.15}$-T (diamond), and $Te_{0.10}Nb_{0.20}$-T (square) sample materials at (A) 300°C, (B) 350°C, and (C) 400°C where ethane conversion was varied by changing residence time at constant ethane and O_2 pressures of 10.13 kPa.

The following figure, Figure 4.3, includes the rate of ethylene formation as a function of ethane conversion. Again, any significant effects of the residence time on product formation rates (product inhibition) were removed by extrapolating all rates measured at $<11\%$ conversions to zero reactant conversion. Therefore, all rates reported reflect ODHE rates at the conditions of the reactor inlet free from all products. All the catalyst samples, except sample $Te_{0.05}Nb_{0.15}$-T, show as ethylene formation increases, the rate of ethane consumption decreases. The initial ethylene formation rate over $Te_{0.05}Nb_{0.05}$-T was about a factor of 13 times greater than the $Te_{0.05}Nb_{0.15}$-T sample and 5 times

greater than the $Te_{0.05}Nb_{0.10}$-T sample. Initial ethylene formation rates decreased as the Nb:Mo molar ratio increased. I propose that increasing Nb content in $(MoVNb)_5O_{14}$ phase catalysts causes Nb to fail to incorporate into the crystalline framework and contributes to the amorphous phase content, decreasing catalytic activity in the ODHE process.

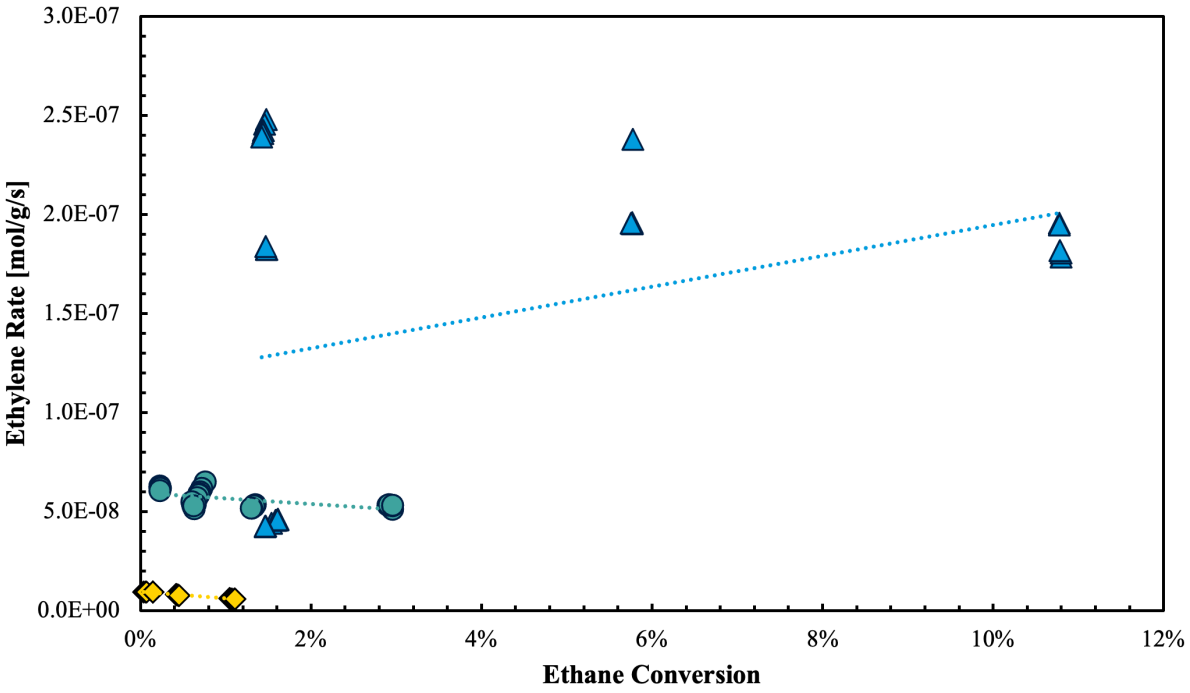

Figure 4.3: Ethylene formation rate as a function of ethane conversion for $Te_{0.05}Nb_{0.05}$-T (triangle), $Te_{0.05}Nb_{0.01}$-T (circle), and $Te_{0.05}Nb_{0.15}$-T (diamond) sample materials at 300°C. Rates were extrapolated to initial residence times (zero reactant conversion) to account for the significant effects of the residence time on product formation rates.

Figure 4.4 depicts the formation rate of the products ethylene, CO_2, and CO at 300°C. Also, all the materials have different rates, which can be attributed to the difference in the V^{5+} active site density. Ethylene formation rate is highest over the $Te_{0.05}Nb_{0.05}$-T sample, while the $Te_{0.05}Nb_{0.15}$-T sample produces the most CO_2. The extreme selectivity to CO_2 of the $Te_{0.05}Nb_{0.15}$-T sample is inconsistent with the idea that Nb spatially isolates the V^{5+} active sites to prevent deeper oxidation of ethylene to CO_2. The percent substitution of Nb in the Mo_5O_{14} framework is not known, but Nb is known to preferentially incorporate into amorphous material. Thus, the assumption that the Mo_5O_{14}-type impurity incorporated high concentrations of Nb into its framework must be invalid.

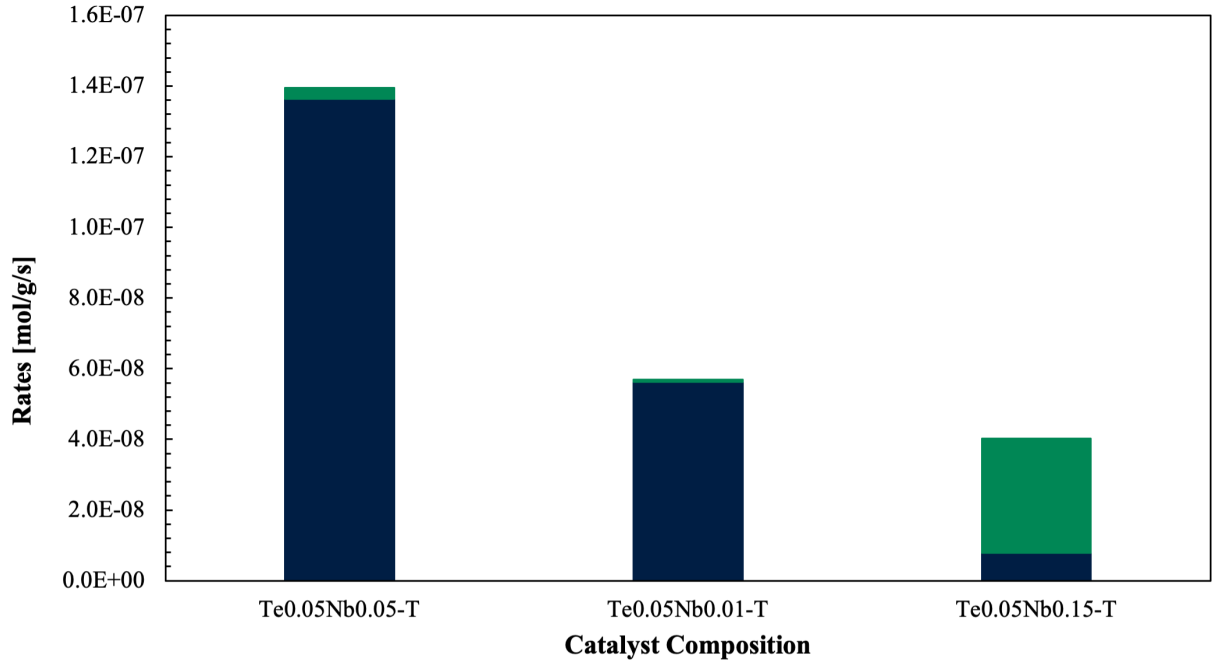

Figure 4.4: Formation rates of ethylene (dark blue) and CO_2 (green) over samples $Te_{0.05}Nb_{0.05}$-T, $Te_{0.05}Nb_{0.10}$-T, and $Te_{0.05}Nb_{0.15}$-T at 300°C.

4.4 Conclusion

Chapter 4 studied the Mo_5O_{14} phase impure materials in the oxidative dehydrogenation of ethane. This chapter analyzed of the tetragonal Mo_5O_{14} phase characterization and its catalytic behavior in the ODHE process. Through X-ray diffraction (XRD) analysis, the Mo_5O_{14} phase was identified alongside other catalyst phases. It was observed that Te and Nb play significant roles in the catalyst's structural and functional characteristics, impacting the overall catalytic performance. The presence of the Mo_5O_{14} phase was marked by low Te contents.

The exploration into the Mo_5O_{14} phase impurities aimed to understand their role and impact on catalytic performance, especially in comparison to the M1 phase discussed in Chapter 3. The samples indicating the presence of the Mo_5O_{14} phase had $\sim$20% lower ethane conversions and formed ethylene at a slower rate compared to the samples containing M1 phase.

Chapter 5

Results and Discussion of Ethane ODH over $TeMo_5O_{16}$ Phase Impure Materials

5.1 Introduction

The partial decomposition of M1 phase and the formation of $TeMo_5O_{16}$, due to increasing Te content, could mask the real surface area of M1 phase and decreasing the specific catalytic activity [30]. To achieve ideal catalytic activity, it is necessary to investigate the impact of Te on monoclinic $TeMo_5O_{16}$ formation. $TeMo_5O_{16}$ has a hexagonal tungsten bronze (HBT)-like crystal structure on the 001 basal plane. The corner-sharing MoO_6 octahedra enclose a hexagonal pore. The tellurite entities form TeO_4 trigonal bipyramid atoms that are connected via oxygen bridges to form infinite chains within the hexagonal pore in the 001 direction. This local environment of Te with the presence of infinite chains makes it similar to the M1 phase [31]. This chapter characterizes the synthesized catalysts using X-ray diffraction (XRD) and reports the catalytic results for the ODHE process over $TeMo_5O_{16}$ impurities.

5.2 Monoclinic $TeMo_5O_{16}$ Phase Characterization

XRD patterns were recorded to understand the relationship between catalyst composition and the formation of different $MoVTeNbO_x$ phases. Phase identification of the catalysts was carried out by comparing the collected spectra with those listed in the ICSD database. Figure 5.1 shows diffraction patterns for the simulated pattern for the reference M1 phase material (ICSD 55097; [25]), Mo5O14 phase material (ICSD 27202; [26]) and $TeMo_5O_{16}$ phase material (ICSD 1081; [32]), as well as samples $Te_{0.20}Nb_{0.05}$-M and $Te_{0.15}Nb_{0.05}$-M after annealing. XRD patterns of samples $Te_{0.20}Nb_{0.05}$-M and $Te_{0.15}Nb_{0.05}$-M suggest the presence of M1, Mo_5O_{14}, and $TeMo_5O_{16}$ phases. The stronger peak intensities of sample $Te_{0.20}Nb_{0.05}$-M corresponds to more ordering along crystal directions (002), (040), (140), (300), (240), (302), and (004). The combination of high Te content and low Nb content must lead to the decomposition of M1 phase into the $TeMo_5O_{16}$ impurity, supporting the idea that excess Te will hinder incorporation into the M1 framework.

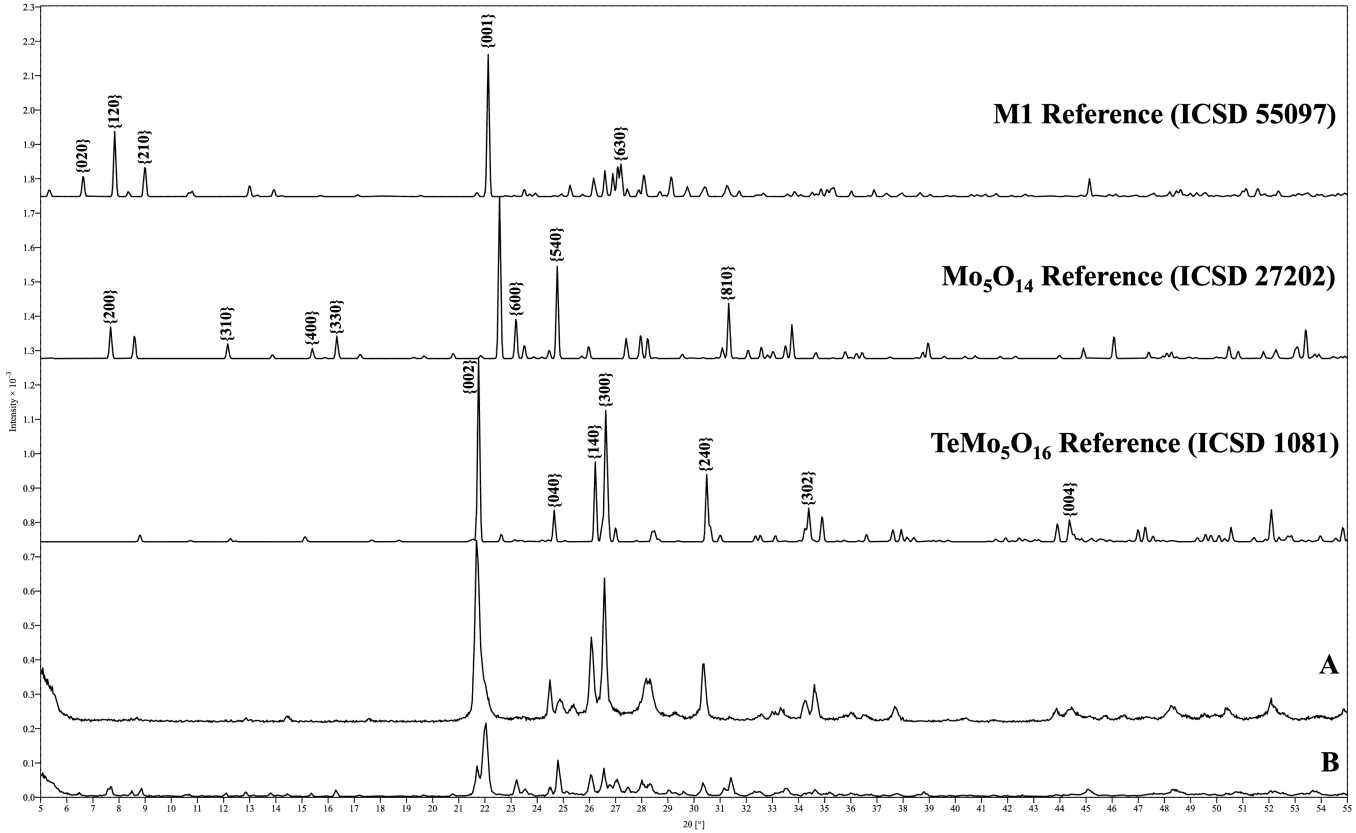

Figure 5.1: XRD patterns of simulated M1 phase (ICSD 55097), Mo_5O_{14} phase (ICSD 27202), and and $TeMo_5O_{16}$ phase (ICSD 1081) as well as annealed $Te_{0.20}Nb_{0.05}$-M (A) and $Te_{0.15}Nb_{0.05}$-M (B) samples from 2θ=5-55°. M1 phase (ICDS 55097) has characteristic diffraction lines located at 2θ = 6.63, 7.83, 8.99, 22.13, and 27.21°, corresponding to the (020), (120), (210), (001), and (630) crystal directions, respectively. Tetragonal Mo_5O_{14}-type structure has characteristic diffraction lines located at 2θ = 7.68, 12.16, 15.40, 16.34, 23.19, 24.77, and 31.34°, corresponding to the crystal directions (200), (310), (400), (330), (600), (540), and (810), respectively. Monoclinic $TeMo_5O_{16}$ structure has characteristic diffraction lines located at 2θ = 21.76, 24.65, 26.23, 26.62, 30.49, 34.38 and 44.36°, corresponding to the crystal directions (002), (040), (140), (300), (240), (302), and (004), respectively.

5.3 Catalytic Results of ODHE Over $TeMo_5O_{16}$ Phase Samples

Following the catalytic tests, ethane conversion, ethylene selectivity, CO_2 selectivity, CO selectivity, and rates were calculated to better understand the effect of Te and Nb content on catalytic activity and selectivity in the ODHE process. Figure 5.2.A plots ethylene selectivity as a function of ethane conversion for $Te_{0.20}Nb_{0.05}$-M and $Te_{0.15}Nb_{0.05}$-M materials at 300°C, where ethane conversion was varied by changing residence time. At low conversions (<3%), both materials exhibit 100% selectivity to ethylene. As conversions increase, selectivities to ethylene decrease slightly. However, the ethane conversion of $Te_{0.20}Nb_{0.05}$-M is higher at 300°C than at 350°C, contrary to the expectation that catalytic activity increases with temperature. At higher temperatures (350°C and 400°C), Figures 5.2.B and 5.2.C show sample $Te_{0.15}Nb_{0.05}$-M has higher ethane conversions and ethylene selectivities compared to $Te_{0.20}Nb_{0.05}$-M. This could be due to the material's closer resemblance to M1 phase than the $TeMo_5O_{16}$. The lower Te content in $Te_{0.15}Nb_{0.05}$-M leads to better Te incorporation into the framework, and the lower amount of $TeMo_5O_{16}$ might expose more M1 surface area for more ideal catalytic activity in ODHE. Additionally, a molar ratio of Te:Mo=0.20 under increasingly sever reaction conditions might cause the Te to reduce from Te^{4+} to form Te^0 on the catalyst surface which blocks the active sites.

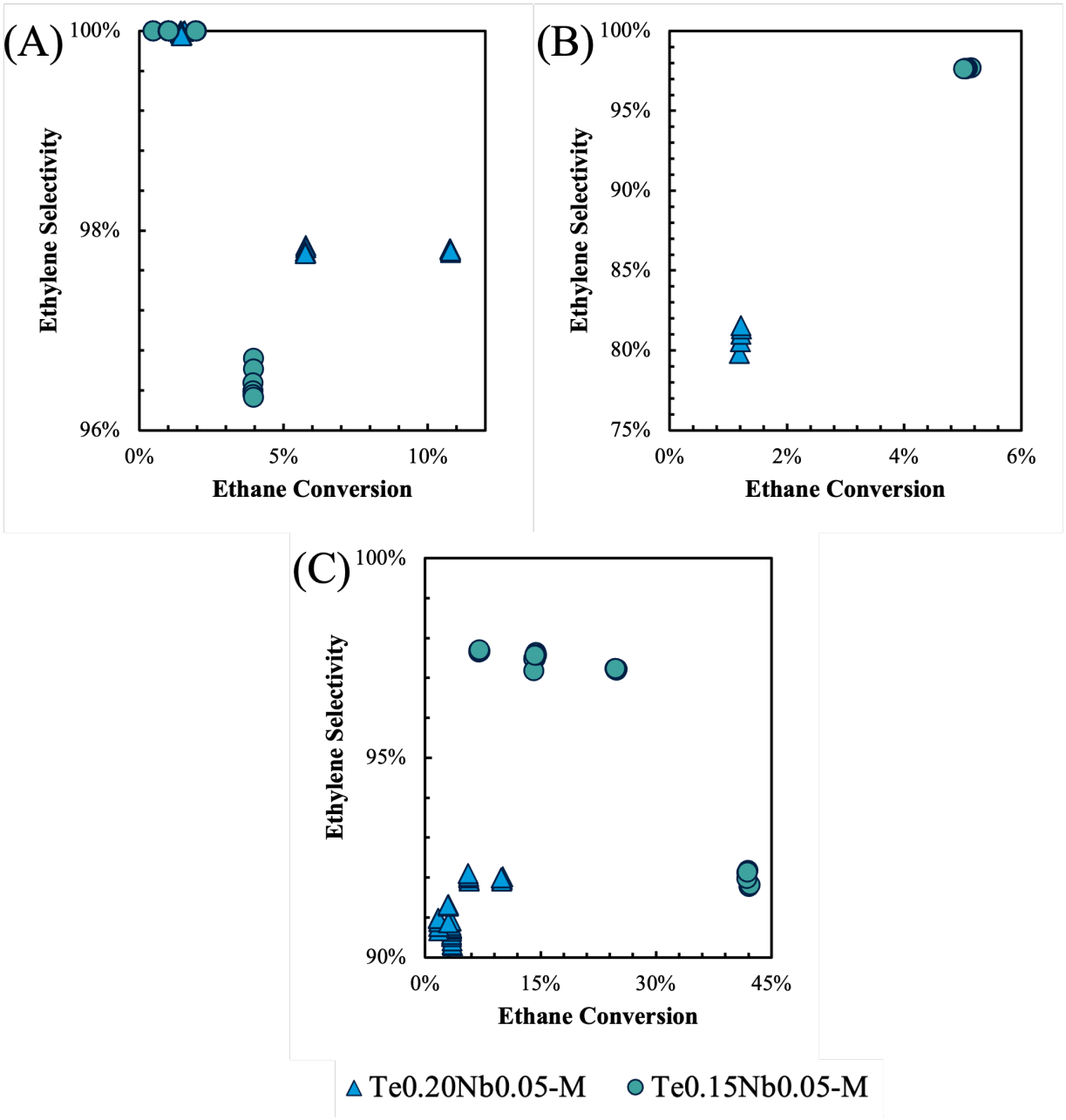

Figure 5.2: Ethylene selectivity as a function of ethane conversion for $Te_{0.20}Nb_{0.05}$-M (triangle) and $Te_{0.15}Nb_{0.05}$-M (circle) sample materials at (A) 300°C, (B) 350°C, and (C) 400°C where ethane conversion was varied by changing residence time at constant ethane and O_2 pressures of 10.13 kPa.

The following figure, Figure 5.3, includes the rate of ethylene formation as a function of ethane conversion. Any effects of significant effects of the residence time on product formation rates (product inhibition) were removed by extrapolating all rates measured at <5% conversions to zero reactant conversion. Therefore, all rates reported reflect ODHE rates at the conditions of the reactor inlet free from all products. Sample $Te_{0.20}Nb_{0.05}$-M follows the trend seen in Chapters 3 and 4: as ethane conversion increases, ethylene formation rate decreases. The opposite is true for the $Te_{0.15}Nb_{0.05}$-M sample. The initial ethylene formation rate of $Te_{0.15}Nb_{0.05}$-M is about a factor of 6

times greater than the $Te_{0.20}Nb_{0.05}$-M sample.

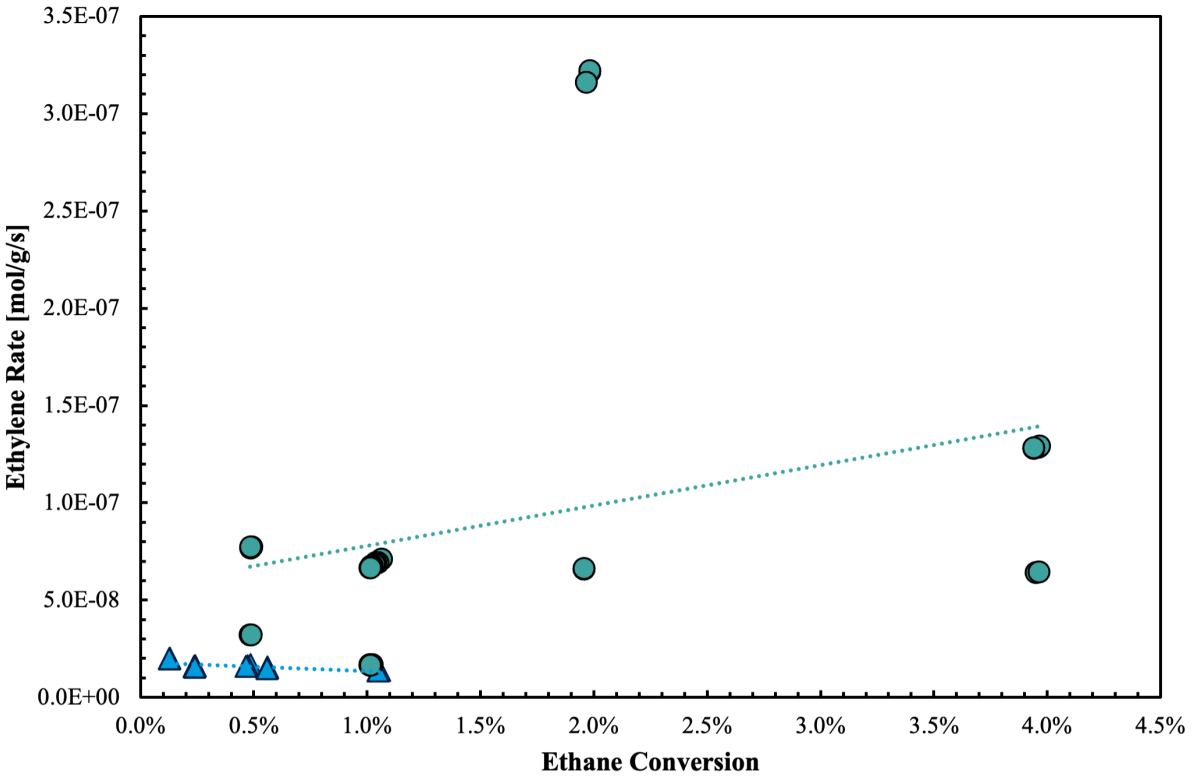

Figure 5.3: Ethylene formation rate as a function of ethane conversion for $Te_{0.20}Nb_{0.05}$-M (triangle) and $Te_{0.15}Nb_{0.05}$-M (circle) sample materials at 300°C. Rates were extrapolated to initial residence times (zero reactant conversion) to account for the significant effects of the residence time on product formation rates.

Figure 5.4 depicts the formation rate of the products ethylene, CO_2, and CO at 300°C. Ethylene formation rate is considerably higher over the $Te_{0.15}Nb_{0.05}$-M sample, while the $Te_{0.20}Nb_{0.05}$-M sample produces more CO_2, supporting the claim that lower Te content leads to better Te incorporation into the framework and lower amount of $TeMo_5O_{16}$ phase formation, which might expose more M1 surface area for more ideal catalytic activity in ODHE.

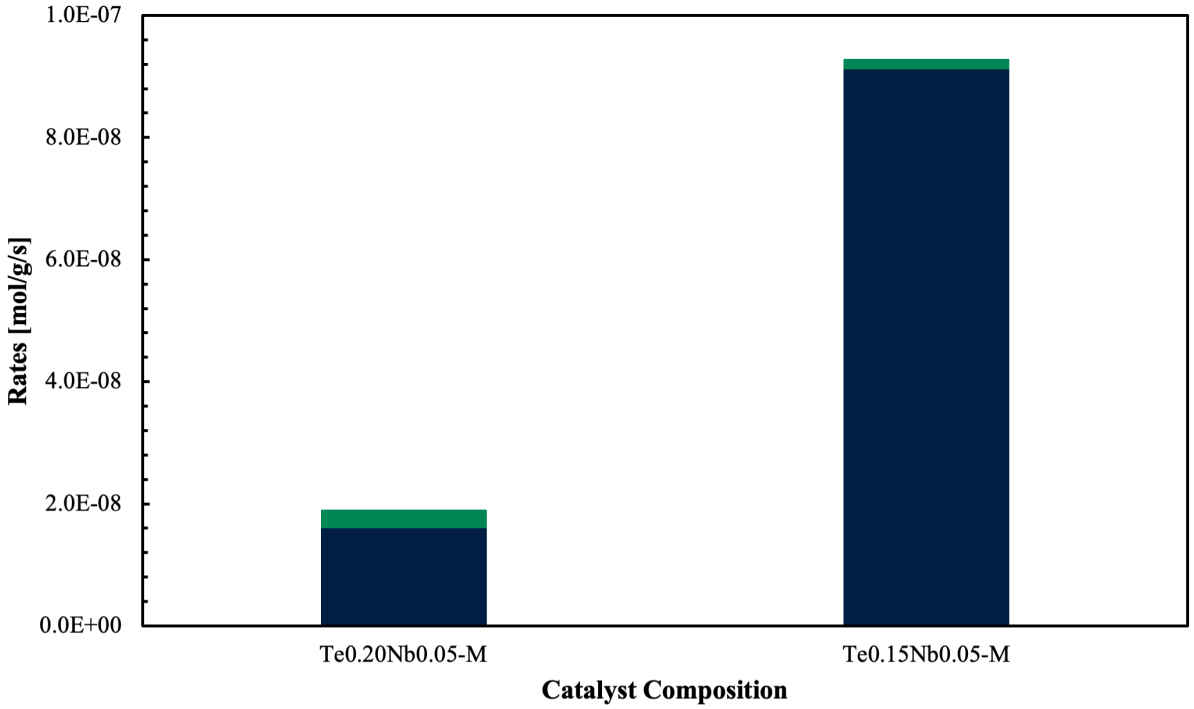

Figure 5.4: Formation rates of ethylene (dark blue) and CO_2 (green) over samples $Te_{0.20}Nb_{0.05}$-M and $Te_{0.15}Nb_{0.05}$-M at 300°C.

5.4 Conclusion

Chapter 5 examined impact of Te and Nb contents on the formation and catalytic performance of monoclinic$TeMo_5O_{16}$ phase impure materials in the oxidative dehydrogenation of ethane. This chapter focuses on the synthesis, characterization, and evaluation of the catalytic performance of materials containing the $TeMo_5O_{16}$ phase, which emerges from the partial decomposition of the M1 phase at increased Te contents. Through X-ray diffraction analysis, the presence of $TeMo_5O_{16}$ phase impurities was confirmed alongside the dominant M1 phase, indicating that the Te content plays a pivotal role in dictating the phase composition of the catalysts. The catalytic performance tests reveal an ideal range of Te content, where excessive Te leads to the formation of the less active $TeMo_5O_{16}$ phase, potentially masking the catalytic sites on the M1 phase and thus hindering overall catalytic efficiency. This phase impurity was shown to significantly influence the activity and selectivity of the catalysts.

The samples with the $TeMo_5O_{16}$ phase performed significantly worse compared to the tetragonal phase impurity and the M1 phase. Both the ethane conversion and ethylene production rates were lower in the $TeMo_5O_{16}$ phase samples than the Mo_5O_{14} phase impurity and M1 phase.

Chapter 6

Conclusions and Future Work

6.1 Conclusion

This thesis presents a comprehensive investigation into the effects of Te and Nb on the catalytic performance of $MoVTeNbO_x$ in the ODHE process. Through XRD and testing catalytic performance, I have shown the incorporation of Te and Nb plays a crucial role in modulating the catalyst's structure and activity. The synthesis process, characterized by specific molar ratios of Te and Nb to Mo, significantly influences the formation of the M1 phase and the Mo_5O_{14} and $TeMo_5O_{16}$ phase impurities, crucial for optimal catalytic activity.

The study finds that a specific Te content (Te:Mo=0.10-0.15) is vital for the formation of the M1 phase without leading to the creation of less active phases such as $TeMo_5O_{16}$. The results suggest that there is an optimal range of Te content that promotes the formation of a phase-pure, highly crystalline M1 phase, which in turn, shows superior catalytic performance in ODHE. Moreover, the presence of Nb is shown to enhance the stability of the M1 phase structure, indirectly affecting the catalyst's selectivity towards ethylene production by spatially isolating active sites and promoting the rapid desorption of the desired products.

The catalytic performance assessments reveal a nuanced understanding of the relationship between catalyst composition, crystallinity, and activity. The findings indicate that catalysts with a Te:Mo molar ratio within a specific range exhibit higher ethane conversion and ethylene selectivity. Furthermore, the study highlights the detrimental effects of excessive Te, leading to the formation of the monoclinic $TeMo_5O_{16}$ phase. This phase impurity exhibited the worst catalytic activity and ethylene selectivities. Whereas the samples indicating presence of the tetragonal Mo_5O_{14} phase reached ethane conversions up to 60% at 400°C, the samples with the monoclinic $TeMo_5O_{16}$ phase just surpasses 40%. In terms of selectivity, the samples with the monoclinic $TeMo_5O_{16}$ phase outperformed the samples with the tetragonal Mo_5O_{14} phase by $\sim$10% despite the lower concentration of Nb. This disagrees with the assumption that all the Nb is able to incorporate in a $(MoVNb)_5O_{14}$ framework. Overall, the M1 phase still performs better in the ODHE process when compared to the impurity phases.

In conclusion, this thesis not only advances our understanding of the complex interplay between catalyst composition, structure, and activity in $MoVTeNbO_x$ catalysts but also lays the groundwork for the development of more efficient catalysts for the oxidative dehydrogenation of ethane. The findings have significant implications for the petrochemical industry, offering pathways to more sustainable and cost-effective ethylene production methods. This research contributes valuable insights into the design and optimization of $MoVTeNbO_x$ catalysts for oxidative dehydrogenation of ethane. It advocates for a deeper understanding of the role of each component in influencing the catalyst's structural and functional characteristics.

6.2 Future Work

6.2.1 Current Materials

Since I did not perform catalytic phase characterization or catalytic performance tests for all synthesized catalyst samples, I would like to test the $Te_{0.10}Nb_{0.05}$-M1, $Te_{0.15}Nb_{0.10}$-M1, $Te_{0.10}Nb_{0.15}$-M1, $Te_{0.05}Nb_{0.20}$-T, and $Te_{0.20}Nb_{0.10}$-M samples phase formation, catalytic activity, and ethylene selectivity. I want to confirm whether the phases and catalytic performance of these compositions

agree with the relationships proposed in this thesis.

6.2.2 Nature of Active Sites

I also would like to perform more characterization tests to understand the effect of Te and Nb on the active sites on the surface of the synthesized catalysts. Mossbauer and XANES tests could help me characterize electronic structures and oxidation state of the Te cations while EXAFS could determine structural information (nature, number, type, local disorder) of neighboring atoms [31]. I would perform each of these techniques before and after the catalyst sample is exposed to reaction conditions.

Additionally, Concepción et al. investigated the active sites in MoVTeNb oxide catalysts during the propane oxidation process [30]. I would like to employ methanol temperature programmed surface reaction (TPSR) spectroscopy and low-energy ion scattering (LEIS) to determine the nature of active surface sites and role of surface cations in $MoVTeNbO_x$ catalysts for the ODHE process [30]. I am specifically interested in studying how Te and Nb content changes the density of active sites on the catalyst of the surface.

To further understand the since the MoVTeNb oxides, I am interested in performing oxygen isotope exchange to identify whether lattice oxygen or adsorbed oxygen species are involved in the ODH of ethane [30]. I want to employ oxygen isotope exchange over the catalyst samples with varying Te and Nb concentrations to reveal how these two elements impact the mobility of oxygen within the catalyst and the stability of the catalyst under reaction conditions/ability of the catalyst to regenerate.

6.2.3 $MoVTeNbO_x$ Catalyst Synthesis and Treatment Methods

Finally, I would like to vary preparation and treatment methods to enhance catalyst performance and stability, potentially leading to more energy-efficient and environmentally friendly processes for ethylene production. For example, I would like to investigate the impact of increasing heat treatment on crystallinity, phase formation, and sublimation of Te in $MoVTeNbO_x$ catalysts. Post annealing at temperatures over 600°C, I would like to perform inductively coupled plasma (ICP) spectroscopy and XRD to determine if the Te content and the phase composition changes. Also, Oliver et al. has prepared Mo-V-Te-Nb mixed oxide catalysts by a slurry method at various pHs and tested these catalysts in the partial propane oxidation to acrylic acid [33]. Recreating this study for the ODHE process might expose how pH influences phase formation and catalytic performance of $MoVTeNbO_x$ catalysts during the ODHE reaction.

Bibliography

[1] Emilia Jackson. US Ethylene Demand Set for Growth in Line with Economic Projections. https://www.chemanalyst.com/NewsAndDeals/NewsDetails/us-ethylene-demand-set-for-growth-in-line-with-economic-projections-243 Jan 2024.

[2] Florian Wéry, Moreno Geerts, Laurien A Vandewalle, Pieter A Reyniers, Geraldine J Heynderickx, Guy B Marin, and Kevin M Van Geem. Assessing the co2 emission reduction potential of steam cracking furnace innovations via computational fluid dynamics: From high-emissivity coatings, over coil modifications to firing control. *Chemical Engineering Research and Design*, 190:129–142, 2023.

[3] Ismaël Amghizar, Laurien A Vandewalle, Kevin M Van Geem, and Guy B Marin. New trends in olefin production. *Engineering*, 3(2):171–178, 2017.

[4] Cheng Zheng, Xiao Wu, and Xianhao Chen. Low-carbon transformation of ethylene production system through deployment of carbon capture, utilization, storage and renewable energy technologies. *Journal of Cleaner Production*, 413:137475, 2023.

[5] SANDRA Wauters and GB Marin. Kinetic modeling of coke formation during steam cracking. *Industrial & engineering chemistry research*, 41(10):2379–2391, 2002.

[6] Vincent N Cavaliere, Marco G Crestani, Balazs Pinter, Maren Pink, Chun-Hsing Chen, Mu-Hyun Baik, and Daniel J Mindiola. Room temperature dehydrogenation of ethane to ethylene. *Journal of the American Chemical Society*, 133(28):10700–10703, 2011.

[7] Yihu Dai, Xing Gao, Qiaojuan Wang, Xiaoyue Wan, Chunmei Zhou, and Yanhui Yang. Recent progress in heterogeneous metal and metal oxide catalysts for direct dehydrogenation of ethane and propane. *Chemical Society Reviews*, 50(9):5590–5630, 2021.

[8] Christian A Gärtner, André C van Veen, and Johannes A Lercher. Oxidative dehydrogenation of ethane: common principles and mechanistic aspects. *ChemCatChem*, 5(11):3196–3217, 2013.

[9] Yuxin Chen, Binhang Yan, and Yi Cheng. State-of-the-art review of oxidative dehydrogenation of ethane to ethylene over movnbteox catalysts. *Catalysts*, 13(1):204, 2023.

[10] Muhammad Numan, Taeho Kim, Changbum Jo, and Sang-Eon Park. Ethane dehydrogenation with co2 as a soft oxidant over a cr-tud-1 catalyst. *Journal of CO2 Utilization*, 39:101184, 2020.

[11] Amin Alamdari, Ramin Karimzadeh, and Saeed Abbasizadeh. Present state of the art of and outlook on oxidative dehydrogenation of ethane: catalysts and mechanisms. *Reviews in Chemical Engineering*, 37(4):481–532, 2021.

[12] Sara Najari, Samrand Saeidi, Patricia Concepcion, Dionysios D Dionysiou, Suresh K Bhargava, Adam F Lee, and Karen Wilson. Oxidative dehydrogenation of ethane: catalytic and mechanistic aspects and future trends. *Chemical Society Reviews*, 50(7):4564–4605, 2021.

[13] Miguel A Bañares. Supported metal oxide and other catalysts for ethane conversion: a review. *Catalysis Today*, 51(2):319–348, 1999.

[14] F Cavani and F Trifiro. The oxidative dehydrogenation of ethane and propane as an alternative way for the production of light olefins. *Catalysis Today*, 24(3):307–313, 1995.

[15] Bozhao Chu, Lara Truter, TA Nijhuis, and Yi Cheng. Performance of phase-pure m1 movnbteox catalysts by hydrothermal synthesis with different post-treatments for the oxidative dehydrogenation of ethane. *Applied Catalysis A: General*, 498:99–106, 2015.

[16] Qi Xie, Luqian Chen, Weizheng Weng, and Huilin Wan. Preparation of movte (sb) nb mixed oxide catalysts using a slurry method for selective oxidative dehydrogenation of ethane. *Journal of Molecular Catalysis A: Chemical*, 240(1-2):191–196, 2005.

[17] Robert K Grasselli, Douglas J Buttrey, Peter DeSanto Jr, James D Burrington, Claus G Lugmair, Anthony F Volpe Jr, and Thomas Weingand. Active centers in mo–v–nb–te–ox (amm) oxidation catalysts. *Catalysis Today*, 91:251–258, 2004.

[18] P Botella, JM López Nieto, B Solsona, A Mifsud, and F Marquez. The preparation, characterization, and catalytic behavior of movtenbo catalysts prepared by hydrothermal synthesis. *Journal of Catalysis*, 209(2):445–455, 2002.

[19] Satoshi Ishikawa, Xiaodong Yi, Toru Murayama, and Wataru Ueda. Heptagonal channel micropore of orthorhombic mo3vox as catalysis field for the selective oxidation of ethane. *Applied Catalysis A: General*, 474:10–17, 2014.

[20] Frederik N Naraschewski, Chinthala Praveen Kumar, Andreas Jentys, and Johannes A Lercher. Phase formation and selective oxidation of propane over movtenbox catalysts with varying compositions. *Applied Catalysis A: General*, 391(1-2):63–69, 2011.

[21] Wataru Ueda, Damien Vitry, and Tomokazu Katou. Crystalline movo based complex oxides as selective oxidation catalysts of propane. *Catalysis Today*, 99(1-2):43–49, 2005.

[22] Robert K Grasselli. Selectivity issues in (amm) oxidation catalysis. *Catalysis Today*, 99(1-2):23–31, 2005.

[23] Wataru Ueda, Damien Vitry, and Tomokazu Katou. Structural organization of catalytic functions in mo-based oxides for propane selective oxidation. *Catalysis Today*, 96(4):235–240, 2004.

[24] R Quintana-Solórzano, G Barragán-Rodríguez, H Armendáriz-Herrera, José Manuel López-Nieto, and Jaime S Valente. Understanding the kinetic behavior of a mo–v–te–nb mixed oxide in the oxydehydrogenation of ethane. *Fuel*, 138:15–26, 2014.

[25] Peter DeSanto Jr, Douglas J Buttrey, Robert K Grasselli, Claus G Lugmair, Anthony F Volpe Jr, Brian H Toby, and Thomas Vogt. Structural aspects of the m 1 and m 2 phases in movnbteo propane ammoxidation catalysts. *Zeitschrift für Kristallographie-Crystalline Materials*, 219(3):152–165, 2004.

[26] L Kihlborg. Crystal structure studies on mo5o14 compound exhibiting 2-dimensional disorder. *Arkiv for Kemi*, 21(5):427, 1964.

[27] Yury V Kolen'ko, Kazuhiko Amakawa, Raoul Naumann d'Alnoncourt, Frank Girgsdies, Gisela Weinberg, Robert Schlögl, and Annette Trunschke. Unusual phase evolution in movtenb oxide catalysts prepared by a novel acrylamide-gelation route. *ChemCatChem*, 4(4):495–503, 2012.

[28] Thommy Ekström. Formation of ternary phases of mo5o14 and mo17o47 structure in the molybdenum-wolfram-oxygen system. *Materials Research Bulletin*, 7(1):19–26, 1972.

[29] Eva Rödel and Thorsten Ressler. *In situ bulk structural investigation of Mo5O14-type mixed metal oxide catalysts for partial oxidation reactions*. PhD thesis, Technische Universität Berlin, 2006.

[30] P Concepción, S Hernandez, and JM López Nieto. On the nature of active sites in movteo and movtenbo catalysts: The influence of catalyst activation temperature. *Applied Catalysis A: General*, 391(1-2):92–101, 2011.

[31] JMM Millet, H Roussel, A Pigamo, JL Dubois, and JC Jumas. Characterization of tellurium in movtenbo catalysts for propane oxidation or ammoxidation. *Applied Catalysis A: General*, 232(1-2):77–92, 2002.

[32] Y Arnaud and J Guidot. Structure cristalline de l'oxyde mixte de molybdène–tellure: Mo5teo16. *Acta Crystallographica Section B: Structural Crystallography and Crystal Chemistry*, 33(7):2151–2155, 1977.

[33] JM Oliver, JM López Nieto, P Botella, and A Mifsud. The effect of ph on structural and catalytic properties of movtenbo catalysts. *Applied Catalysis A: General*, 257(1):67–76, 2004.

Appendix

6.3 Constants and Calculations

To analyze the GC chromatograms, a python script was written to extract the FID and TCD peak areas and tabulate the values. Based on the reference retention times [minutes] (Table 6.1) and peak areas [pA*s and 25 μV*s] from the FID and TCD, respectively, the FID detected methane, ethane, and ethylene while the TCD detected methane, ethane, ethylene, O_2, N_2, CO_2, and CO. The peak areas measured by the FID were normalized (Equation 6.1) based on the number of carbons in each compound and response factors (Table 6.2):

$$\text{Normalized Area} = \frac{(\text{Peak Area})}{\text{Number of Carbons} \cdot \text{Response Factor}} \tag{6.1}$$

Approximate Retention Times For Each Species	
FID	
Methane	1.6 min
Ethane	1.9 min
Ethylene	2.7 min
O_2 and N_2	1.1 min
CO	5.1 min
TCD	
CO_2	1.6 min
Ethylene	6.7 min
Ethane	7.2 min

Table 6.1: Approximate retention times for each analyte determined from reference the chromatographs provided by each column

Compound	Response Factors
Hydrocarbons (FID)	1567.9 area/kPa
CO (TCD)	905.8 area/kPa
CO_2 (TCD)	1231 area/kPa
Ethylene (TCD)	1065.1 area/kPa
Ethane (TCD)	1065.1 area/kPa
Methane (TCD)	840 area/kPa

Table 6.2: Experimentally determined response factors for FID and TCD

The peak areas derived from the TCD were solely divided by the response factor. The total area for the FID was the sum of the normalized areas of methane, ethane, and ethylene, and the total area from the TCD was the sum of the normalized areas of methane, ethane, ethylene, O_2, N_2, CO_2, and CO.